Modelling and control of a hydraulic servo system

$\mathcal{H}_\infty$ control and LPV control versus classical control

F.P. Wijnheijmer

DCT Report no: 2005.90

TU/e Master Thesis
14th June 2005

Supervisors:
prof.dr.ir. M. Steinbuch
dr. ir. W.J.A.E.M. Post
ir. P.C. Teerhuis

University of Technology Eindhoven (TU/e)
Department of Mechanical Engineering
Division Dynamical Systems Design
Control System Technology group

Abstract

This thesis examines the modelling and control of a hydraulic servo system. Both a theoratical and a practical approach are discussed. The used set-up consists of an one DOF hydraulic system with an electronically controlled servo valve. A nonlinear parametric model of the system, several fitted linear black box models as well as a LPV model combining these fits are determined. The models are verified with the use of experimental data.

Combining position and pressure feedback, classical hydraulic controllers, $\mathcal{H}_\infty$ controllers and a LPV controller are designed to control the position of the rod. The design of the controllers takes into account several aspects of the system's dynamics like the damping effect of pressure feedback and the nonlinear characteristics dependent on the position of the rod. The controllers are implemented using an analogue control board as well as a discrete dSpace system. In discretisation of the control strategies for implementation on a discrete dSpace system, a new algorithm is derived for LPV structures. Simulations and experimental results indicate the benefits of a variable controller over a classical controller, but show the limitations to this strategy as well.

This reports concludes with the suggestion that the next step in researching servo hydraulic actuators, is the combination of hydraulic servo control and mimo systems. For this purpose, a two DOF hydraulic system with varying dynamic interaction between the DOF's is designed and built. To facilitate the design of a mimo controller, MCDesign is developed, a tool for mimo controller design based on measurements data from a mimo system.

Samenvatting

Dit verslag beschrijft de modellering en control van een hydraulisch servo systeem. Hiervoor is een een DOF hydraulische cylinder gebruikt met een electronisch gestuurde hydraulische servo klep. Van dit systeem zijn verschillende modellen gemaakt. Eerst is er een parametrisch model gemaakt, dit is vergeleken met een op meetwaarden gefit black box model. Van dit black box model is met behulp van de kennis uit het parametrische model een LPV model gemaakt.

Op basis van deze modellen zijn controllers ontworpen met zowel positie als druk terugkoppeling. Er zijn conventionele hydraulische controllers, $\mathcal{H}_\infty$controllers en een LPV controller ontworpen en getest. Het ontwerp van deze controllers omvat zowel het dempende effect van de druk terugkoppeling als het niet lineaire gedrag van de hydraulische cylinder. De controllers zijn getest met behulp van een analoge regelkast en met een digitaal dSpace systeem. Om ook de LPV controller discreet te kunnen implementeren is een nieuw discretisatie algoritme geschreven voor LPV systemen. De uitgevoerde simulaties en experimenten geven een goed overzicht van de voor- en nadelen van de verschillende geavanceerde controller in vergelijking met de conventionele technieken.

Dit verslag sluit af met de suggestie dat de volgende stap in een onderzoek naar hydraulische systemen, is de combinatie van hydraulisch servo control en mimo systemen. Hiertoe is een twee DOF hydraulisch servo systeem ontworpen en gebouwd met varirende interactie tussen de twee vrijheidsgraden. Om het ontwerp van een mimo controller te vereenvoudigen, is MCDesign ontwikkeld. Dit is een tool om mimo controllers te ontwerpen gebaseerd op meetdata van mimo systemen.

Nomenclature

Var	Description	Value	Unit
Modelling			
V	Oil volume in the cylinder	$0 \dots A \cdot L$	m^2
A	Piston Area	$19.6 \cdot 10^{-4}$	m^2
L	Stroke length	$2 \cdot 10^{-3}$	m
E	Oil bulk modulus	$1 \cdot 10^{9}$	Pa
m	Mass of load	130	kg
y	Position of load	$0 \dots 200$	mm
$\dot{y}$	Speed of load		mm^{-1}
$\ddot{y}$	Acceleration of load		mm^{-2}
$\dddot{y}$	Jerk of load		mms^{-3}
u	Electric voltage to the current amplifier		V
i	Electric current to the servo valve		A
p	Oil pressure in the cylinder	$0 \dots p_s$	Pa
p_s	Supply pressure	$70 \cdot 10^5$	Pa
p_L	Load pressure	$-35 \cdot 10^5 \dots 35 \cdot 10^5$	Pa
p_n	Normalised load pressure	$-1 \dots 1$	[-]
q_N	Nominal oil flow through the valve	$0.63 \cdot 10^{-3}$	m^3s^{-2}
q_v	Normalised oil flow through the valve	$-1 \dots 1$	[-]
$q_{N_{leak}}$	Nominal leakage flow over the piston		m^3s^{-2}
q_{leak}	Leakage flow over the piston		m^3s^{-2}
x	Valve spool position	$-1 \dots 1$	[-]
F	External force on load		N
X_n	Valve spool position (Laplace transformed)		
Y	Load position (Laplace transformed)		
P	Load pressure (Laplace transformed)		
U	Input voltage (Laplace transformed)		
Linearising			
x_0	Mean valve spool position		[-]
x_e	Variations around mean valve spool position		[-]
p_0	Mean load pressure		[-]
p_e	Variations around mean load pressure		[-]
Control			
H	System		
H_y	Position transfer function		
H_p	Pressure transfer function		
$H_{y_{damp}}$	Position transfer function damped by pressure feedback		

continued on next page

continued from previous page

Variable	Description	Value	Unit
C	Controller		
C_{pos}	Position controller		
C_{press}	Pressure controller		
$\mathcal{H}_\infty$ and LPV Control			
P	Plant		
C	Controller		
S	(output) Sensitivity		
T	Complementary sensitivity (Closed loop)		
CS	Control sensitivity		
SP	Process sensitivity		
r	Tracking reference		
e	Tracking error		
v	Control output		
r	System input		
w	Disturbance signal		
V_r	Reference signal filter		
V_u	Plant uncertainty filter		
V_η	Noise level filter		
W_e	Tracking error filter		
W_u	Control output filter		
γ	Infinity norm of augmented plant		
θ	Dependency parameter LPV models		

Preface

This thesis is written within the framework of a graduation project for the Master of Sience Degree in Mechanical Engineering at the Eindhoven University of Technology. Trying to combine theory and practice at the one hand and hydraulics and control at the other hand, electro hydraulic servo control is a good base for a multi disciplinary graduation project.

On the one hand, the assignment consists of the modelling of a hydraulic system and the understanding of the hydraulic practise. On the other hand it consists of the challenge to see the hydraulic system as a controllable system and to find a (suitable) controller. Both modelling and control are performed in theory and are tested on an actual hydraulic test set-up. In addition to this, a new set-up is designed for further research on other aspects of the hydraulic control problem.

In the first chapter an introduction to the problem and its place in a greater context is given. Part 1 describes the modelling of the system. This paret is devided in two chapters. Chapter 2 describes a physical white box model of the system and chapter 3 describes a measurement based black box model. The control aspect is discussed in part 2. This consists of three chapters each describing another control approach. The design of the new set-up is explained in chapter 7. Chapter 8 presents the conclusions and recommendations.

Contents

Chapter 1

Introduction

1.1 A hydraulic motion system

Electro hydraulic actuators can apply high forces and have a high power-to-volume ratio, partly because, next to actuating, these actuators can also be used as construction elements. Furthermore they have a great robustness against their surrounding environment. With this in mind, the use of electro hydraulic actuators in flight simulators, robots, tele-controlled manipulator etcetera is an obvious choice. Koekebakker [2001] describes the design of a hydraulic actuated flight simulator. Sugiyama & Uchida [2002] describe a hydraulic actuated injection moulding process and the research program of Rexroth [2005] also reveals a variety in hydraulic applications.

Comparing these applications reveals that all these systems consists of a kinematic multi-input-multi-output (mimo) systems with multiple electo hydraulic controller actuators. A disadvantage of these systems, however, is the significant nonlinear behaviour of the hydraulic actuators [Merrit 1967; Viersma 1990; Post & Teerhuis 2005]. Since modern control strategies can more and more deal with non linear behaviour, this advantage can be compensated. Recently, this has resulted in a renewed interest in electro hydraulic servo controlled motion systems.

Yun & Cho [1988] and Yao et al. [1999] propose the use of adaptive control to cope with the non-linearities in the hydraulic actuators. They use the adaptation however in a situation where the non-linearities are known beforehand. So Sohl & Bobrow [1999] use a force-based control strategy to come to a sort of dynamic feedback linearisation [Sastry 1999]. Although the results are promising, it merely shifts the nonlinear control problem to the force controller than that it really solves the problem. Sirouspour & Salcudean [2000] are able to cope with the nonlinearity using back stepping resulting in input linearisation of the hydraulic system.

Using a gain scheduling control strategy, a controller that has the capability to vary for varying parameters can be found. Wassink et al. [2005] use such a strategy to control an injection moulding machine. Linear parameter varying control (LPV control) uses robust control approach as a basis to come to a gain scheduling controller with proven stability [Scherer & Weiland 2005; Sugiyama & Uchida 2002].

1.2 Problem definition

Considering the above, two basic questions can be formulated before designing a mimo hydraulic actuated system:
1) What is the best strategy to control a hydraulic actuator?
2) How does this influence the control of a mimo hydraulic system with coupled dynamics?

To answer the first question, this thesis focuses on the modelling and control of a single-input-

single-output (siso) hydraulic servo system. Both modelling and control strategies are verified on an actual hydraulic test set-up. The modelling consists of a physical model and of a model based on frequency domain measurements. The control consists of a comparison of a number of controllers. An $\mathcal{H}_\infty$ controller and an LPV controller [Damen & Weiland 2002; Scherer & Weiland 2005] are compared with a classical hydraulic controller [Viersma 1990; Post & Teerhuis 2005]. To answer the second question a mimo system is designed and built based on available actuators. This system has two degrees of freedom with varying dynamic interaction actuated by two hydraulic cylinders. The results of this research indicates which control strategies are worth investigating in further research for the mimo system.

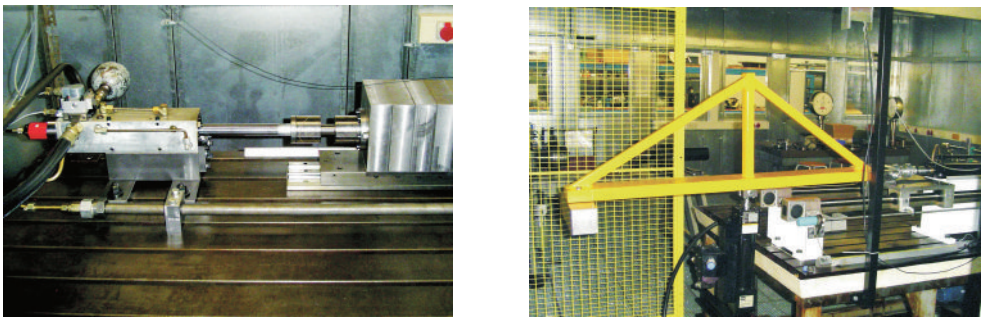

a **b**

Figure 1.1: **a**: The siso hydraulic set-up used in the control design in this thesis, **b**: the mimo hydraulic set-up designed and built for further research.

1.3 Siso set-up

The siso hydraulic servo system used for this research consists of an asymmetric hydraulic actuator and a servo valve (See chapter 2.1). A schematic overview of the hydraulic system and the interaction between the various elements is shown in Figure 1.2.

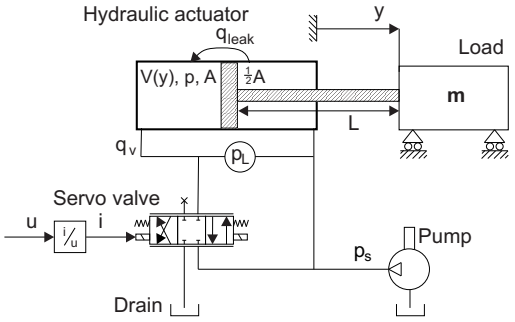

Figure 1.2: Schematic overview of the hydraulic system with the servo valve, the hydraulic cylinder and the external load.

A mass of 130 kg is moved horizontally by a single rod double acting hydraulic actuator. A elctro hydraulic servo valve on top of the cylinder controls the oil flow to the cylinder. The valve is placed close to the actuator to minimise the 'dead' oil volume between the valve and the actuator. This ensures fast responses. The position of the system is defined as the position of the load and is measured in the cylinder rod. The pressure difference over the cylinder is measured between the valve and the actuator.

The actuator is an asymmetric hydraulic actuator with hydrostatic bearings. (See section 2.1.1). The actuator was built at the Delft University of Technology. The actuator has a stroke of 200 mm, a piston surface of $9.8 \cdot 10^{-4}$ mm^2 at the rod side and $19.6 \cdot 10^{-4}$ mm^2 at the piston side. (The actuated side, see section 2.1). The mass is a mounted on a linear guide to protect the cylinder's bearings.

The position sensor is a MTS Temposonic sensor [see MTS 2005]. It consists of a rod (a so called wave gide) in the rod, with a circular magnet around it attached to the piston . If the rod moves, the magnet also moves along the waveguide. A magnetic pulse is send from the head of the transducer through the waveguide. This magnetic pulse initiates a strain pulse in the waveguide at the magnet's position according to the Lorenz principle. This momentum pulse travels through the waveguide back to the transducer's head with a sonic speed. The time difference between the magnetic pulse and the momentum pulse is measured and transferred to an analog signal between -10 V and 10 V. The pressure sensor is a Paine differential pressure sensor [see Paine 2005]. It measures the pressure difference between the supply line and the control line. It has an analog output that is amplified. This results in a pressure signal with a range of -10 V and 10 V. The electro hydraulic servo valve is a MOOG 76-233 high speed type of of control valves [see MOOG 2005].

1.4 Mimo set-up

Viersma [1990] shows that a hydraulic set-up has significant nonlinear behaviour. This can be researched with the siso set-up. Most hydraulic applications consists of multiple degrees of freedom that also introduces nonlinear behaviour. To be able to experiment with a 2-dof hydraulic system, a system is designed and built that includes all these factors. The system is designed so that in one working point no coupling exists between the degrees of freedom. In other operating points coupling does exist. Figure 1.3 shows three different layouts proposed for such a system. All three layouts have one translating dof and one rotating dof. This is done to make the construction of the system more easy. Two translating dofs require more guidance and two rotational dofs cause make mounting the second dof hydraulic actuator difficult. All three layouts have coupled dynamics. However, only in layouts (b) and (c) does movement in one direction does cause acceleration in the other direction. This applies for both dofs. Layout (c) is the only layout where the actuators act differently on the system for different working points. As layout (c) has all mimo factors in its design, this layout is chosen.

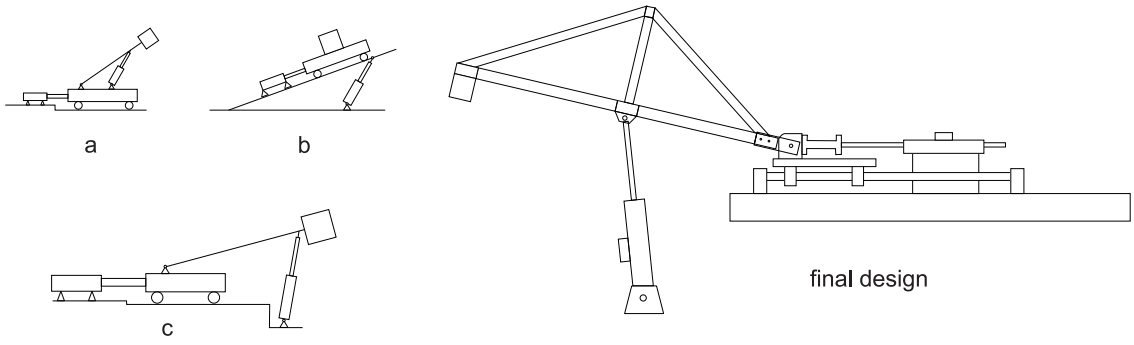

Figure 1.3: Three proposed designs and the final design

Part I

Modelling

Chapter 2

White box Model

To gain more knowledge of the behaviour of the system, this part describes the system identification and modelling. System models can be divided into white box models and black box models. First, a white box model is made by modelling the parts of the system based on their physical behaviour. This model is used to gain a better understanding of the behaviour of the system. This chapter describes the physical white box modelling . Also, a black box model is made, which is is described in chapter 3. This model is based on a frequency domain fit of measured transfer functions of the system. During the fitting procedure some knowledge of the white box model is taken into account. Finally the white box model is fitted on the measurements by changing its parameters in accordance with the parameters in the black box model.

2.1 White box modelling

The first part of the modelling consists of the derivation of a physical model of the system. This model is called a white box model. The model is based on a physical description of the different parts of the hydraulic system. In modelling the hydraulic system the three main parts, the servo valve, the hydraulic actuator and the external mechanics are taken into account. The sensors of the system, including a differential pressure transducer between the valve and the cylinder [Paine 2005] and a position sensor (a MTS Temposonic) [MTS 2005] are assumed to be ideal and therefore not taken into account in the white box modelling.

2.1.1 Hydraulic actuators

The hydraulic actuator used in the set-up is an asymmetric cylinder with hydrostatic bearings (See Figure 2.1). Two types of cylinders exist: symmetric and asymmetric cylinders. This is short for respectively, double acting, single rod cylinders and double acting, double rod cylinders. A symmetric cylinder has a rod at both sides of the piston and is actuated by applying oil pressure at one of the ports of the piston. An asymmetric piston has a rod only at one side, so the piston areas are different at the opposite sides. Such a cylinder is connected as depicted in Figure 1.2. The valve only regulates the flow to one port of the cylinder. The supply pressure from the pump acts at the other port of the cylinder. This supply pressure retracts the piston with a force of $\frac{1}{2}A \cdot p_s$, so a controlled pressure of $\frac{1}{2}p_s$ at the other port of the cylinder will hold the cylinder into place. The load pressure ($p_L = p - \frac{1}{2}p_s$), is the resulting pressure working on the load $p_L \in [-\frac{1}{2}p_s, \frac{1}{2}p_s]$. The load pressure is normalised (see eq. 2.1).

$$p_L = p - \frac{1}{2}p_s$$

$$p_n = \frac{1}{\frac{1}{2}p_s} p_L \qquad \in [-1, 1] \tag{2.1}$$

The cylinder has hydrostatic bearings. This means that the piston has a conical clearance between the piston and the cylinder. A pressure difference over the piston will push some oil through this conical clearance that works as a bearing. Such a piston has very low friction as it actually floats in the cylinder. This set-up introduces a leak flow q_{leak} from the one side of the piston to the other side.

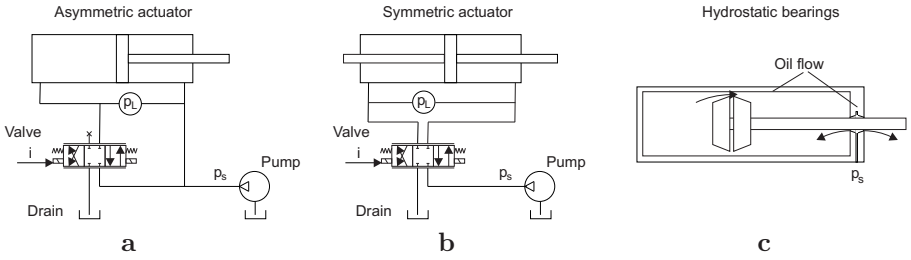

Figure 2.1: Plot a: a symmetric actuator. Plot b: an asymmetric actuator. Plot c: Hydrostatic bearings.

The leak flow is also normalised using the maximum leak flow ($q_{N_{leak}}$). Since the used actuator is an asymmetric actuator, the maximum leak flow occurs if zero pressure is applied by the servo valve. In that case no pressure acts at the actuated side of the piston and the full supply pressure acts at the other side of the piston. This situation corresponds to a normalised load pressure $p_n = -1$. The leak flow that occurs in that situation is regarded as $q_{N_{leak}}$. The leakage is assumed to be laminair [Merrit 1967,p.132]. This gives a liner relationship between the pressure difference and the leakage (see eq. 2.2).

$$q_{leak} = \frac{1}{2} q_{N_{leak}} (1 - p_n) \tag{2.2}$$

To derive a model for the hydraulic actuator a flow balance for the cylinder chambers [Merrit 1967,p.132] is used. This flow balance describes the piston movement as function of the oil flow from the valve to cylinder (q_v), the oil leakage (q_{leak}) and the oil volume difference as function of the pressure difference. This results in the following model of the cylinder (see eq. 2.3).

$$\begin{aligned} A\dot{y} &= -\frac{V}{E}\dot{p_L} + q_v + q_{leak} \\ \dot{p_n} &= \frac{2E}{p_s V}\left(q_v - A\dot{y} + \frac{1}{2} q_{N_{leak}} (p_n - 1)\right) \end{aligned} \tag{2.3}$$

As follows from eq. 2.3, the volume $V{=}A \cdot y$ influences the dynamics of the cylinder. This means the dynamic behaviour changes during movement of the rod, which indicates nonlinear behaviour. This will be a major issue during controller design.

2.1.2 Servo valves

A great variety of hydraulic valves exists and servo valves form a small part of that variety. Servo valves are valves that can dynamically regulate the oil flow through the valve in a proportional manner. Figure 2.2 shows a picture of a typical servo valve. If a current i is applied at the torque motor, the T-formed flapper rotates slightly in the plane of the figure due to the induced momentum. Now at one side of the flapper, the offset between nozzle and flapper increases

slightly, which decreases the hydraulic resistance in that nozzle. This results in an increased oil flow through the nozzle that causes a pressure drop in the connected control line. The resulting pressure difference in the control lines causes the spool to move. This movement bends the feedback spring, which applies a counter acting momentum on the torque motor and makes the nozzle openings become equal again. This way, the feedback spring makes a feedback loop. This makes displacement of the spool linear dependent on the rotation of the torque motor. So the spool displacement becomes linear dependent on the current.

The displacement of the spool creates a gap between the pressure line and one of the control lines and it creates a second gap between the tank and the other control line.

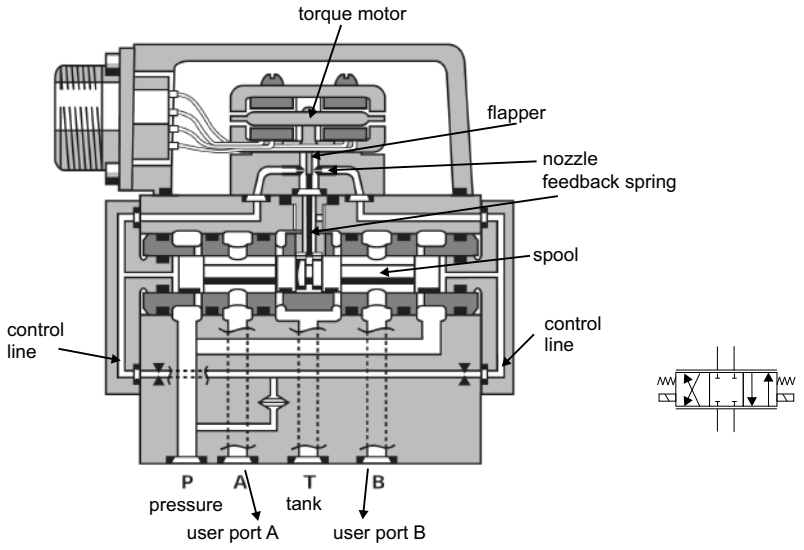

Figure 2.2: A electrohydraulic servo valve of MOOG GmbH

Different types of these valves exist. Main difference is in the spool land configuration in the servo valve. A valve has overlap when the spool has to move a small distance from its centre before a gap is created. A valve has underlap when all gaps are open slightly if the valve is in its centre position. A valve is called critical centre if no gap is open in the centre position, but every small displacement will open a gap. The valve used in the setup used in this research is a critical centre valve. In the set-up only one control line is used that results in connection of the valve depicted in Figure 1.2.

The mechanical feedback loop makes the low frequent displacement of the spool (or the valve opening) linear dependent to the electric actuation current of the motor. The dynamic behaviour of the feedback spring and the spool dominates the dynamic behaviour of the servo valve. This behaviour is provided by the supplier by means of a transfer function for a certain volume flow through the valve (see Figure 2.3).

The valve is actuated by means of an electric current. This current is generated by a current amplifier. This amplifier is supposed to be ideal so the transfer from the input voltages to the output current is one. In practise, this means that the transfer function from current to spool displacement is equal to the transfer function from voltage to spool displacement. So the mentioned transfer function provided by the supplier can be used as transfer function from input voltage to spool displacement. These dynamics are modelled using a 2^{nd} order filter (see eq. 2.4).

$$\frac{X_n}{U} = \frac{1}{c_1 s^2 + c_2 s + 1} \tag{2.4}$$

The constants of eq. 2.4 are fitted using Figure 2.3. Attention is paid to the fitting of the phase

rather than the amplitude as the phase lag is most important in control design [Franklin et al. 1993].

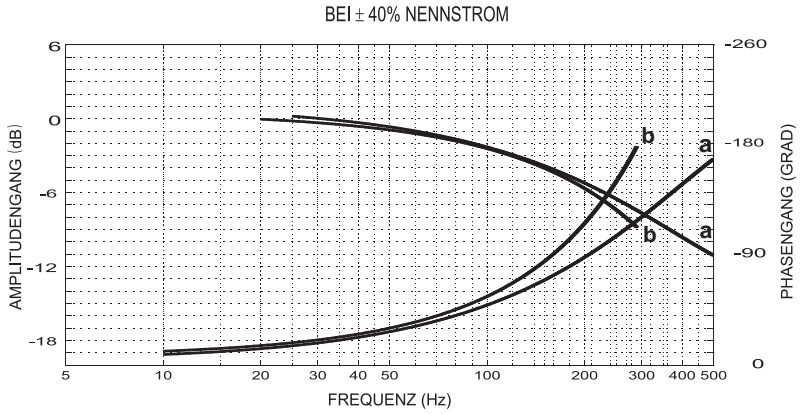

Figure 2.3: Transfer function of the applied critical centre electrohydraulic servo valve, MOOG 76-233 [MOOG 2005].

The dynamics of the servo valve depends on the volume flow through the valve. So the valve dynamics are nonlinear. The supplier gives the dynamic behaviour of the serve valve at various volume flows. In this research the volume flows are considered to be below 40% of the maximum flow. This assumption can be made since no fast movements are made. So in this research the servo valve is considered to be linear. The transfer function for the dynamic behaviour of the servo valve is based on the data supplied for a volume flow of 40% of the maximum volume flow.

2.1.3 Flow through the valve

If the servo valve is actuated, the oil pressure causes a flow through the small orifice of the spool. These local flow characteristics are the base of the general valve behaviour. Servo valves are designed to have a turbulent flow through a orifice. This means that the flow is proportional to the square root of the pressure drop over the valve: $q \propto \sqrt{\Delta p}$. Depending on the opening direction of the valve, this formula results in the following equations:

$$q = \begin{cases} \propto \sqrt{p_s - p} & = q_N x \sqrt{1 - p_n} \quad x > 0 \\ & 0 \qquad\qquad\quad x = 0 \\ \propto \sqrt{p_s + p} & = q_N x \sqrt{1 + p_n} \quad x < 0 \end{cases} \tag{2.5}$$

with eq. 2.1 $\left(p_n = \frac{2}{p_s}\left(p - \frac{1}{2}p_s\right)\right)$, and q_N the nominal flow, which is the oil flow for a maximal valve opening and a pressure difference over the servo valve of $70 \cdot 10^5$ Pa. The value of q_N is provided by the supplier. This nonlinear equation for the flow through the valve is linearised around $(x_0, p_0) = (\epsilon, 0)$. No static external force is applied to the system, so the pressure is linearised around zero. Equation 2.5 is only valid for a turbulent flow. This does not exist if the valve is closed, so the equation is linearised around a small valve opening. Furthermore, a small valve opening will always exist when a controller is actuating the system.

$$\begin{aligned} q &= q_N x \sqrt{1 - \frac{|x|}{x} p_n} \\ q_{lin} &= \left.\frac{\delta q}{\delta x}\right|_{(x,p_n)=(x_0,p_{n_0})} x_e + \left.\frac{\delta q}{\delta p}\right|_{(x,p_n)=(x_0,p_{n_0})} p_e \end{aligned} \tag{2.6}$$

$$\begin{aligned} &= q_N\sqrt{1-\frac{|x|}{x}p_{n_0}}x_e - \frac{|x|}{x}\frac{q_N x_0}{2\sqrt{1-\frac{|x|}{x}p_{n_0}}}p_{n_e} \\ &= q_N\left(x_e - \frac{|x|}{x}\frac{\epsilon}{2}p_{n_e}\right) \end{aligned} \tag{2.7}$$

If a static force is applied to the system, for instance if the cylinder is used to lift a mass, the pressure should be linearised around a small value of p_0. If the equation is linearised around $(x_0, p_0) = (\epsilon, p_0)$ the equation becomes:

$$q_{lin} = q_N\left(Cx_e - \frac{|x|}{x}\frac{\epsilon}{2C}p_n\right) \text{ with: } C = \sqrt{1-\frac{|x|}{x}p_0}$$

The system described in the thesis is placed horizontally so gravitation forces do not have an effect on the system. Furthermore, no static force are applied at this system so eq. 2.7 will be used.

2.2 External mechanics

The position of the rod is influenced by the external mechanics connected to the rod. In this case, the load is a mass on a horizontal guide with negligible friction (see eq. 2.8).

$$\begin{aligned} F &= m\ddot{y} \\ m\ddot{y} &= \frac{p_s}{2}Ap_n \\ p_n &= \frac{2m}{Ap_s}\ddot{y} \end{aligned} \tag{2.8}$$

2.3 The overall set-up

Substituting eq. 2.3, 2.7 and 2.8 yields the dynamic model of the total system except for the servo valve (see eq. 2.9).

$$\frac{mV}{EA^2}\dddot{y} + \frac{m}{A^2p_s}(q_{N_{leak}} + q_N\epsilon)\ddot{y} + \dot{y} = \frac{q_N}{A}x \tag{2.9}$$

To gain a better understanding of these dynamics, eq. 2.8 and 2.9 are transformed to the frequency domain using a Laplace transformation. This results in the eq. 2.10 and 2.11 for the position transfer functions and for the pressure transfer functions:

$$\frac{Y}{X_n} = \frac{c_3}{s(c_4s^2 + c_5s + 1)} \tag{2.10}$$

$$\frac{P_n}{X_n} = c_6s^2\frac{Y}{X_n} \tag{2.11}$$

with:

$$c_3 = \frac{q_N}{A} \quad c_4 = \frac{m}{EA^2}Ay \quad c_5 = \frac{m}{A^2p_s}(q_{N_{leak}} + q_N\epsilon) \quad c_6 = \frac{2m}{Ap_s} \tag{2.12}$$

As the volume V is linearly dependent on the displacement of the rod, the parameter c_4 is also linearly dependent on this displacement. This results in one position-dependent complex pole pair. Furthermore the position transfer function (eq. 2.10) has an integrating action while the pressure transfer function (eq. 2.11) a differentiating action (see Figure 2.4).

The dynamics of the servo valve (eq. 2.4) still must be added to eq. 2.10. If the valve is fast enough, this extra dynamics have little effect on the system. In this case, however, the valve has a relatively large phase lag that has a considerable effect on the system. Therefore the two poles of the valve model must be added to the system dynamics (see Figure 2.4). The actual values of the system parameters are provided in the nomenclature. This results in the eq. 2.13 and 2.14 for the position transfer function and the pressure transfer function:

$$\frac{Y}{U} = \frac{1}{c_1 s^2 + c_2 s + 1} \frac{c_3}{s(c_4 s^2 + c_5 s + 1)} \tag{2.13}$$

$$\frac{P_n}{U} = c_6 s^2 \frac{Y}{U} \tag{2.14}$$

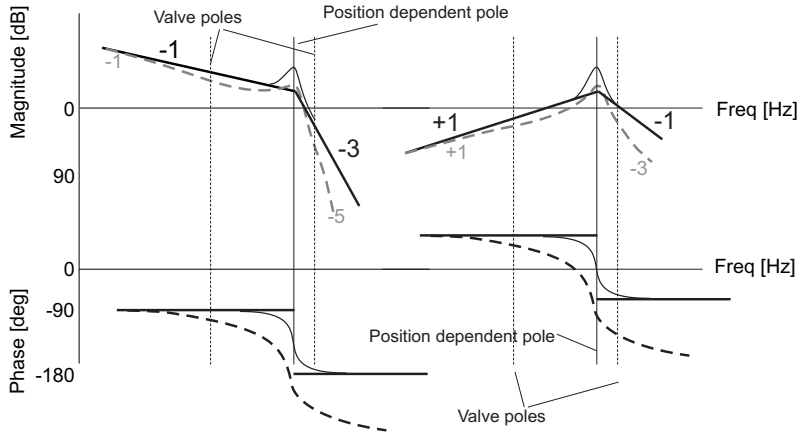

Figure 2.4: Poles and zeros resulting from the white box modelling. The solid line represents the hydraulic system without the servo valve. The thick lines are the systems asymptotes and the thinner lines represents the system itself. The dashed line represents the system including the valve dynamics.

2.4 Conclusion

In this chapter a white box dynamical model is derived for the system. This is represented in the format of a parametric model. This model consists of the dynamics of the servo valve, the hydraulic actuator and the load. The servo valve dynamics are based on a fit on information from the supplier. The hydraulic actuator dynamics are linearised around zero load pressure and a small valve opening. The load is modelled as a single mass. No friction is modelled between the load and its guiding. This results in a 5^{th} order model for both the transfer from the input voltage to the position of the system and the the transfer from the input voltage to the pressure of the system. The model is dependent on the rod position of the system.

Chapter 3

Black box model

Next part of the modelling, is the comparison of the white box model with measurements on the system. Frequency response estimates of the system are fitted. These fits form the black box models. The parameters used in these fits, combined with some extra measurements can be used to fit the white box model parameters onto the actual system. Transfer function estimates of input-output measurements are used to determine the input-output behaviour of the system and develop a black box model. The white box model indicates that the system has a moving complex pole pair for different rod positions (see eq. 2.3). Consequently a set of transfer functions at various positions of the rod (linearisation points) is determined.

3.1 Measurement fits

Two commonly used techniques to determine the transfer function of a system are a sensitivity measurement or a direct measurement. In the direct method, the output y and the input u are measured (see Figure 3.1) and the division of the fourier transformated signals of y over u, results in the transfer function estimate of the system H.

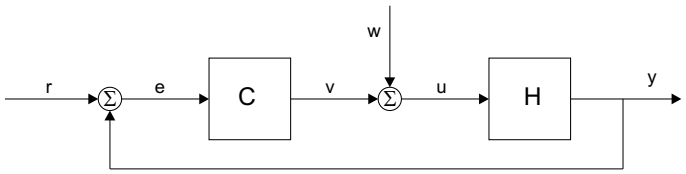

Figure 3.1: Schematic representation of the set-up for the measurement of the transfer functions of the system H.

A sensitivity measurement can be used if a weak feedback loop is required to stop the system from drifting. This method is also more robust to measurement noise. In that case the sensitivity is determined by calculating the transfer function estimate from a disturbance signal w to the control signal u (see Figure 3.1). The system H can be calculated from the sensitivity S, as represented by eq. 3.1.

$$S = (I + HC)^{-1} \tag{3.1}$$

The coherence function between w and u, is a measure how well the output power is a function of the input power. This is a measure for the accuracy of the measurement. For the actual set-up, as discussed in the paper, the direct measurement method gives the best results for the

pressure transfer function and the sensitivity measurement gives the best results for the position transfer. So with these techniques, measurements are performed at the following four rod positions: $y \in 10, 50, 100, 190$ mm. The positions are chosen non linear since the natural frequency is a function of $\frac{1}{y}$ (see 2.10). Figure 3.2 and 3.3) show a plot of the measurements used for the black bx fit.

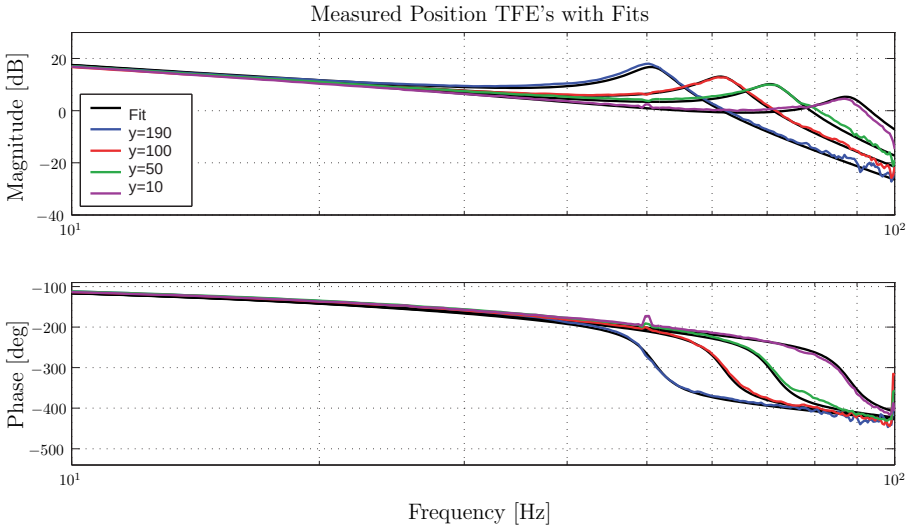

Figure 3.2: Position transfer function estimate.

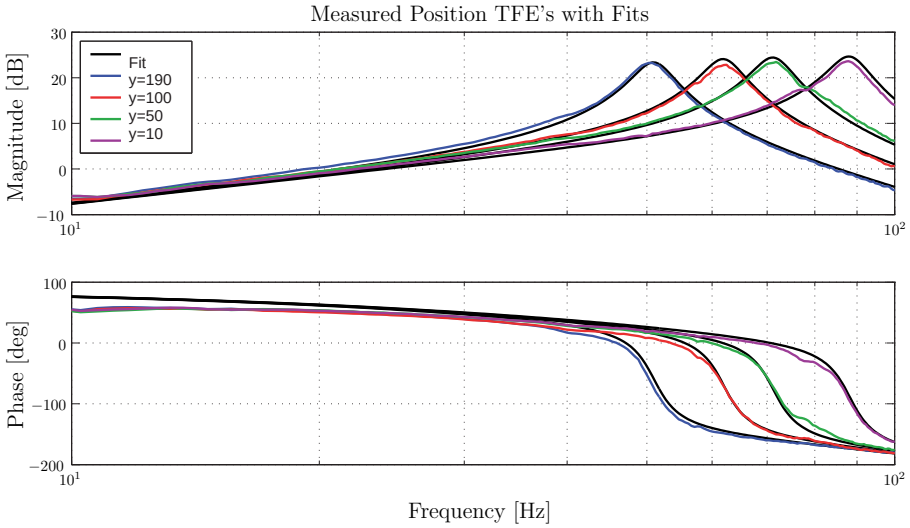

Figure 3.3: Pressure transfer function estimate.

3.1.1 Pole zero fit in MCDesign

Using pole-zero placement, four models are fit on the for position transfer functions and four models on the pressure transfer functions. These fits are subjected to certain restrictions formulated in chapter 2. The number of poles and zeros and their mutual relationship is derived from Figure 2.4. This means that the position fits have a varying complex pole at the natural frequency, 2 fixed poles for the valve dynamics and an integrating action. The pressure fits have the same complex

pole, 2 fixed poles for the valve and sensor dynamics and a differentiator (see Figure 3.2 and 3.3). Since no good mimo pole zero fit procedures is available that can discount the formulated restrictions, the fits are made manually with a tool called `MCDesign.m` [MCDesign 2005]. First, a siso fit is made of the four position transfer functions and the four pressure transfer functions using a least squares algorithm in Matlab, called `FrFit.m` [DIET 2005]. The resulting models are all loaded into separated instances of the MCDesign tool. With this tool the poles and zeros of the fits can be shifted to make the various models match onto each other.

In comparison to the white box model, an extra fixed pole at about 45 Hz is required to fit the position transfer functions. This is likely to be the result of the position sensor dynamics. This is verified by calculating the transfer function from the input signal to the acceleration of the system measured with an extra acceleration measurement. These transfer functions do not show this extra pole (see Figure 3.4). The extra pole is possibly caused by an analog filter in the position sensor. The sensor is equipped with an internal analog filter that prevents high frequent signals from the sensor to intrude in the analog output signal of the sensor.

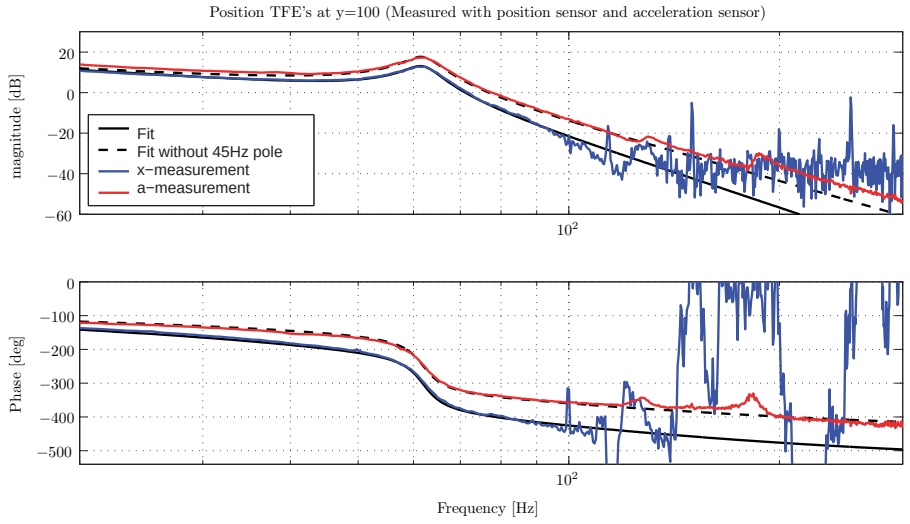

Figure 3.4: Comparison of the position transfer function estimate based on the position sensor and based on the acceleration sensor.

This results in 4 zero-pole-gain models for the position transfer functions and, four model for the pressure transfer. This means that 4 models are derived each consisting of two fitted transfer functions.

3.2 Linear parameter varying model

Anticipating at the development of a Linear parameter varying controller (or LPV controller) (chapter 6), a LPV model is derived using the black box models of section 3.1. The LPV model is a state space representation with matrix entries that can vary linearly in a parameter θ [see Voort et al. 2003].

$$\begin{aligned} \dot{x} &= A(\theta)x + B(\theta)u \\ y &= C(\theta)x + D(\theta)u \end{aligned}$$

With: x: the states of the model, y: the outputs of the model, u: the inputs of the model and θ: the varying parameter.

Two types of LPV models exist: affine models and polytopic models. Affine models describe the varying matrices as $A(\theta) = A_0 + \theta A_1$ and polytopic describe matrices as $A(\theta) = \theta_1 A_1 + \theta_2 A_2$. These two descriptions are of course by transferred into each other. As Matlab's LPV algorithm gives output in the polytopic form, this form is chosen to describe the system.

The LPV model is based on the 4 black box models for $y \in \{10, 50, 100, 190\}$ mm, since those represent the system most accurate. Therefore these transfer functions are rewritten in state space models. This is done in steps to ensure that the valve and sensor dynamics appear apart from the cylinder dynamics in the state space system and to ensure that both the position and the pressure transfer function will have the same A matrix. This is accomplished by transferring the systems step by step to state space. The first step is to make 4 state space systems consisting only of the varying complex pole pair (H_{a_1} till H_{a_4}). The second step is to make a state space system that consists of the static poles of the position transfer (H_b) and a state space system that consists of the static poles of the pressure transfer (H_c). H_c has both a pole and a zero at 45 Hz. This ensures that the A-matrix of H_b and H_c are the similar, but that H_b has actually an extra pole compared to H_c. The third step is to scale H_b and H_c to make their A-matrix equal. The H_b and H_c can be joined to a-one-input-two-output state space system (H_d). Now $H_d H_{a_1}$ till $H_d H_{a_4}$ are the 4 state space representations of the 4 black box models.

These four systems have only 3 entries in the A-matrix that are unequal for the four systems. These are the stiffness and damping of the shifting natural frequency and the gain between the valve dynamics and the dynamics of the natural frequency. These three parameters also can be found in the white box model. For the white box model eq. 2.9 is derived, which can be rewritten in:

$$\dddot{y} = \frac{q_N E A}{mV} x - \frac{E}{p_s V}(q_{N_{leak}} + q_N \epsilon)\ddot{y} - \frac{EA^2}{mV}\dot{y} \tag{3.2}$$

With $\mathbf{x} = [y\ \dot{y}\ \ddot{y}]$ and $\mathbf{u} = [x]$ this gives following state space description:

$$\dot{\mathbf{x}} = \begin{bmatrix} 0 & 1 & 0 \\ 0 & 0 & 1 \\ 0 & \frac{C_1}{V} & \frac{C_2}{V} \end{bmatrix} \mathbf{x} + \begin{bmatrix} 0 \\ 0 \\ \frac{C_3}{V} \end{bmatrix} \mathbf{u} = A(V)\mathbf{x} + B(V)\mathbf{u} \tag{3.3}$$

with: $C_1 = -\frac{E}{p_s}(q_{N_{leak}} + q_N \epsilon)$, $C_2 = -\frac{EA^2}{m}$ and $C_3 = \frac{q_N E A}{m}$. Note that if this equation is multiplied with the valve dynamics, $\frac{C_3}{V}$ als becomes part of the greater A-matrix.

This depicts how the three entries vary with the position. Since $V = Ay + V_0$ (with V_0 the volume in the cylinder for a fully retracted rod position), these matrices are a linear function of $\frac{1}{Ay+V_0}$. When also the valve dynamics and the pressure transfer function are taken into account, these three varying entries all appear in the new larger A-matrix.

By introducing a parameter $\theta \in [0 \cdots 1] \propto \frac{1}{y+c_a}$ this A-matrix can be rewritten as a linear combination of two matrices: $A = A_0 + \theta A_1$. Since $c_a = V_0/A$, c_a is equal for all three entries. So c_a is first fitted for all entries. Then the three varying matrix entries are fitted as a linear function of θ using a least squares solution (see eq. 3.4).

$$\theta = \frac{c_b}{y + c_a} + c_c \tag{3.4}$$

The constant c_a is chosen so that it minimises this least squares error (see Figure 3.5).

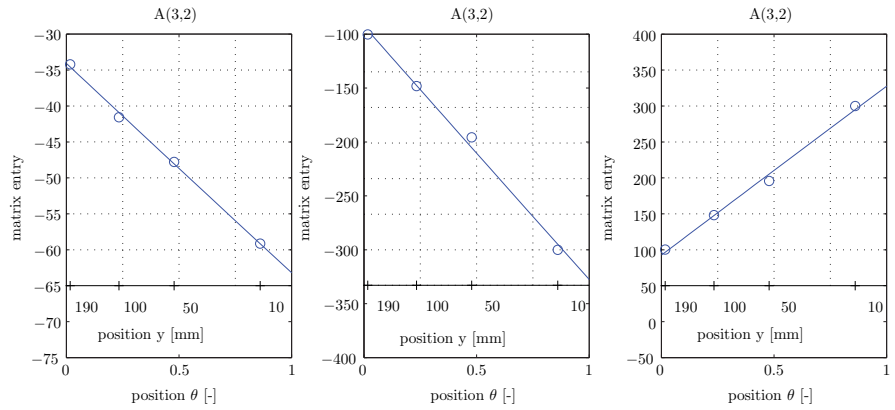

Figure 3.5: The fit of the three varying entries of A.

This results in the LPV model for the plant in the affine structure $A_0 + \theta A_1$. This system is transferred to a polytopic model $A = \theta A_1 + (1-\theta)A_2$. (see eq. 3.5). As the system is velocity actuated, it has a free body mode. This can cause problems during controller design using the LPV algorithm. So finally, to prevent potential numerical problems, an small amount of extra stiffness is added between the the system and the fixed world. This results in the LPV model in eq. 3.5 and depicted in Figure 3.6.

$$\begin{aligned} \dot{\mathbf{x}} &= (\theta A_1 + (1-\theta)A_2) \cdot \mathbf{x} + B \cdot \mathbf{u} \\ \dot{\mathbf{y}} &= C \cdot \mathbf{x} + D \cdot \mathbf{u} \end{aligned} \tag{3.5}$$

3.3 White box model fitted onto the black box model

The black box model poles and zeros are used to fit the white box model in the frequency domain. The white box model is linearised and written as a separate position and a pressure transfer function. During the black box modelling one pole is added to model the position sensor dynamics. If that pole is also added to the white box model transfer function, both models have the same number of poles and zeros. Now the white box parameters can be compared with the poles and zeros of the black box model. There is, however, one problem with the fitting of those parameters: the model has more parameters than just poles and zeros. This means that more measurements have to be made in order to fit all the parameters.

Some values are provided by the supplier, for example the cylinder area $A = 19.6 \cdot 10^{-4}$ mm^2, the mass $m = 130$ kg, the nominal flow $q_N = 0.63 \cdot 10^{-3}$ m^2/s, the supply pressure $p_s = 70 \cdot 10^5$ Pa and the stroke of $L = 200$ mm. Other parameters must be determined by other measurements on the system. Such measurements are based on the following equations (derived in the paper as eq. 3.8 till 3.12)

$$q_{lin} = q_N \left(x - \frac{|x|}{x} \frac{\epsilon}{2} p_n \right) \tag{3.6}$$

$$\dot{p_n} = \frac{2E}{p_s V} \left(q - A\dot{y} - \frac{1}{2} q_{N_{leak}} (p_n - 1) \right) \tag{3.7}$$

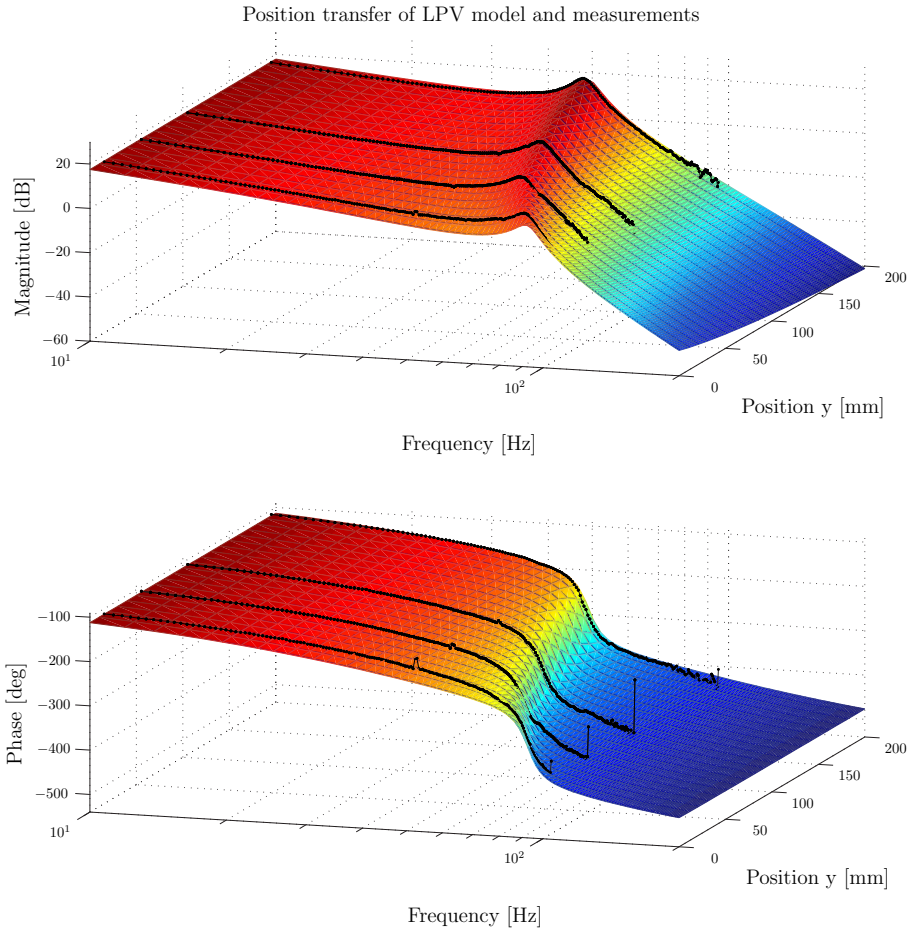

Figure 3.6: 3D Bode diagram of the LPV model. To compare the LPV model with the measurements, the measured transfer functions are also plotted on top of the model.

$$p_n = \frac{2m}{Ap_s}\ddot{y} \tag{3.8}$$

$$\frac{mV}{EA^2}\dddot{y} + \frac{m}{A^2p_s}(q_{N_{leak}} + q_N\epsilon)\ddot{y} - \frac{q_{N_{leak}}}{2} + \dot{y} = \frac{q_N}{A}x \tag{3.9}$$

These equations can be rewritten as transfer functions:

$$\frac{X_n}{U} = \frac{1}{c_1s^2 + c_2s + 1} \tag{3.10}$$

$$\frac{Y}{U} = \frac{c_3}{s(c_4s^2 + c_5s + 1)}\frac{1}{c_7 + 1}\frac{X_n}{U} \tag{3.11}$$

$$\frac{P_n}{U} = c_6s^2\frac{Y}{U} \tag{3.12}$$

3.3.1 Transfer functions

The constants c_3 till c_7 can be derived from the poles and zeros from the black box model (c_1, c_2 and c_7 are also modeled as two constants in the white box model). This results in the following

equations:

$$c_3 = \frac{q_N}{A} \qquad c_4 = \frac{m}{EA^2}Ay \qquad c_5 = \frac{m}{A^2 p_s}(q_{N_{leak}} + q_N\epsilon) \qquad c_6 = \frac{2m}{Ap_s} \quad (3.13)$$

From the black box model the following values are found for these constants: $c_3 = 0.472$, $\frac{c_4}{y} = [3.3 \cdot 10^{-4} \cdots 9.9 \cdot 10^{-5}]$, $c_5 = [2.0 \cdot 10^{-4} \cdots 3.3 \cdot 10^{-4}]$ and $c_6 = 0.014$.

The manufacturers of the valve and the cylinder state that $q_N = 6.3 \cdot 10^{-4}$ m^2/s and $A = 19.6 \cdot 10^{-4}$ m^2. This would lead to $c_3 = 0.32$. This deviation is caused by the gain between the controller output in Volts and the valve input in Ampère and equals to 0.74.

With c_6, A and p_s, the mass m can be calculated as 96 kg. This is less than the estimated mass of 130 kg. The error is most probably caused by a wrong estimation of the value for p_s. For a pressure $p_s = 100 \cdot 10^5$ Pa, the mass would have been 130 kg.

The values for c_4 and c_6 vary for different fits. This indicates some errors in the fits. Other measurements, described further on, show that these values are within a acceptable range.

To estimate other parameters of the white box model and to verify the described parameters, additional measurements are performed.

3.3.2 Constant flow

The acceleration $\ddot{y}$ and the pressure p_n are zero, if the valve opening is constant $\dot{x} = 0$ and no external forces act on the system. Eq. 3.7 now becomes:

$$\dot{y} = \frac{q_N}{A}x + \frac{1}{2A}q_{N_{leak}} \quad (3.14)$$

This relationship can be verified by an experiment. The valve is set to different positions and both valve position and velocity are averaged over time, when the velocity is approximately constant. Figure 3.7 shows these results and a linear fit through the measurements. The valve position cannot be measured, but the current to the valve is assumed to be linear to this position. The slope in the figure equals 0.25 and the offset equals $7 \cdot 10^{-4}$. The slope of the fit in the figure shows that $\frac{q_N}{A} = 0.25$. As stated in sec. 3.3.1 This value should be 0.32 and the difference is caused by the amplifier gain of .7. From the offset, the leakage can be calculated: $q_{N_{leak}} = 7 \cdot 10^{-4} \cdot 2A = 2.74 \cdot 10^{-6}$ m^2/s, which is approximately 0.5% of q_N.

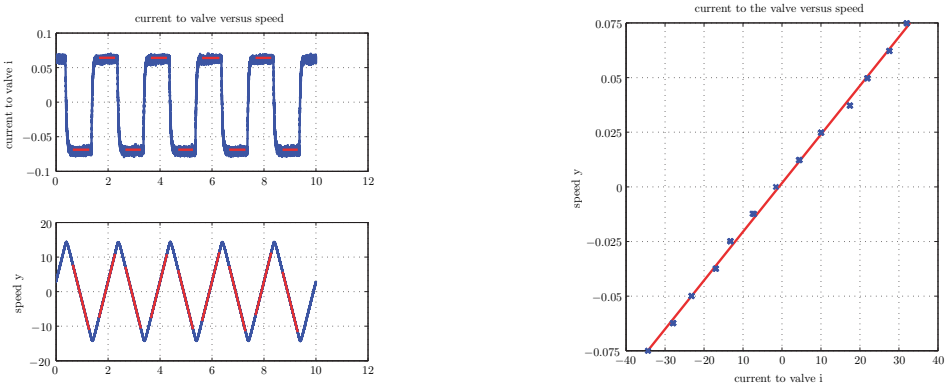

a **b**

Figure 3.7: **a:** In the upper figure, valve openings are plotted in time. In the lower figure the corresponding speeds are plotted. **b:** Rod speed versus valve position. The blue dots are measurements, the red line is a least squares fit.

3.3.3 Fixed rod

If the rod is hold in a fixed a position, $\dot{y}$ and $\dot{p_n}$ become zero. In which case, substituting the below reprinted equations 2.3 and 2.7,

$$\begin{aligned} q_{lin} &= q_N \left(x - \frac{|x|}{x} \frac{\epsilon}{2} p_n \right) \\ \dot{p_n} &= \frac{2E}{p_s V} \left(q - A\dot{y} - \frac{1}{2} q_{N_{leak}} (p_n - 1) \right) \end{aligned}$$

give:

$$q_N x - q_N \frac{|x|}{x} \frac{\epsilon}{2} p_n = \frac{1}{2} q_{N_{leak}} (p_n - 1) \tag{3.15}$$

$$x = \left(\frac{q_{N_{leak}}}{2q_N} + \frac{|x|}{x} \frac{\epsilon}{2} \right) p_n - \frac{q_{N_{leak}}}{2q_N} \tag{3.16}$$

with: $\frac{1}{C_H} = \left(\frac{q_{N_{leak}}}{2q_N} + \frac{|x|}{x} \frac{\epsilon}{2} \right)$ the hydraulic stiffness, this can be simplified to:

$$p_n = C_H x + \frac{C_H q_{N_{leak}}}{2q_N} \tag{3.17}$$

Since q_{lin} is linearised around a spool position ($x = \epsilon$) and a pressure ($p_n = 0$), this linear relationship between x and p_n only holds for small variations around $x = \epsilon$ and $p_n = 0$. Since the spool displacement cannot be measured, the current to the valve is used as a position estimate.

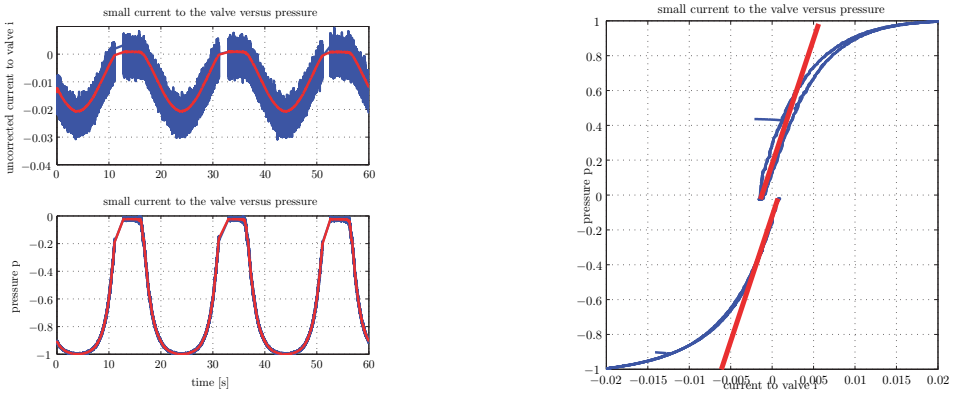

a **b**

Figure 3.8: **a:** In the upper figure, a small fluctuating current to the valve is plotted in time. In the lower figure the corresponding pressure differences are plotted. **b:** Hydraulic stiffness. The blue line is the relationship between a small current to the valve i and the cilinder pressure p_n. The red line is the slope around $x = 0$.

This relationship can be verified with an experiment. First, the rod is put in its most extended position. The valve is actuated with a small positive current. The current to the valve and the pressure are measured. Second, the same experiment is repeated for a fully retracted rod position and small negative current to the valve. Figure 3.8 shows the results of this experiment. The slope of the red line is $C_H = 143$. The measured x should be corrected for the gain of the current amplifier. After correction the slope of the red line appears to be $C_H = 185$. With

$q_{N_{leak}} = 0.5\% q_N$ from the previous experiment, the value of ϵ can be calculated: $\epsilon = 6.5 \cdot 10^{-3}$, which is approximately 0.6% of the maximum valve opening.

The discontinuity in the pressure lines can be explained by the leakage. The leakage makes the rod to extend when the valve is closed. So a small negative valve displacement is required to stop the rod from moving outward. At the most extended position, the rod cannot be extended further, so no valve displacement is required to stop the rod from moving. The measured offset of 0.3 and the value of $\frac{C_H q_{N_{leak}}}{2 q_N}$ (0.45) are of the same order.

The resulting values of the system parameters are listed in table 3.1:

Table 3.1: Measured system parameters

variable		value
$q_{N_{leak}}$	(leak flow)	0.5% q_N m^2/s
p_s	(pressure)	$70 \cdot 10^5$ Pa
ϵ	(valve opening for linearising)	0.6% x_{max}
C_H	(hydraulic stiffness)	185% x_{max}
provided by supplier:		
L	(stroke)	0.2 m
A	(cylinder Surface)	$20 \cdot 10^{-4}$ m^2
m	(mass)	130 kg
q_N	(nominal flow)	6.33 m^2/s
assumed:		
E	(bulk modulus)	$1 \cdot 10^9$ Pa

3.4 Conclusion

In this chapter the black box model is derived for the system. 8 zero-pole-gain models are fitted on 8 measured position and pressure transfer function estimates. These fits are made for rod positions of 10, 50, 100 and 190 mm. From these fits 4 state space models are derived. These state space systems only differ from each other in one moving complex pole pair. From the state space models a single LPV model is made. This model is position dependent. This results in a 6^{th} order model for the system that has a position-dependent complex pole pair that varies between values of 50 till 90 Hz.

Besides, using these fits and some additional measurements the parameter values for the white box model are derived.

Part II

Control design

Chapter 4

Classical hydraulic control

The aim of this part is to compare different feedback strategies for the discussed hydraulic servo system. Although the use of feedforward controllers can improve performance, feedforward design is not considered, as the focus lies on the comparison of feedback strategies. The design of the controllers is based on the linearised models derived in chapter 2. The only non-linearity that is taken into account, is the shifting of the complex-pole pair of the position-dependent natural frequency of the system. This varying complex-pole pair has a significant influence on the control design, as the controller should be sufficiently robust for variations in this complex-pole pair. The aims for the control design are smooth position tracking and sufficient disturbance rejection for the highest possible bandwidth. With this in mind, different control strategies are compared.

4.1 Control set-up

Three different types of controller are designed for the system. First, the classical hydraulic approach is described as a benchmark for the other controllers. This approach consists of proportional position feedback, with additional pressure feedback to damp the natural frequency of the system [see Viersma 1990; Post & Teerhuis 2005]. In this approach, a controller is tuned for the system in the position that gives the lowest natural frequency. In other positions, the higher natural frequency of the system leads to increased phase margin. So the controller will also be stable for other positions. Secondly, a more general approach is regarded to find a controller that is sufficiently robust for the variations in the natural frequency. An $\mathcal{H}_\infty$ controller is derived that is robust for specific variations in the natural frequency. Thirdly, to find a controller that can adapt to the variations in the natural frequency, a Linear Parameter Varying (LPV) controller is derived.

4.2 Description of the control problem

To design a controller, first the model of the system is examined. The system consists of a combination of a highly damped 4^{th} order system and a 2^{nd} order system with a shifting complex pole pair. To increase the bandwidth of the system some D-action can be added to increase the phase of the 4^{th} order system. To increase the bandwidth further, the natural frequency of the 2^{nd} order system should be shifted to a higher frequency with a notch filter. Figure 4.1 shows that the implementation of a notch filter is difficult as the natural frequency of the 2^{nd} order system shifts.

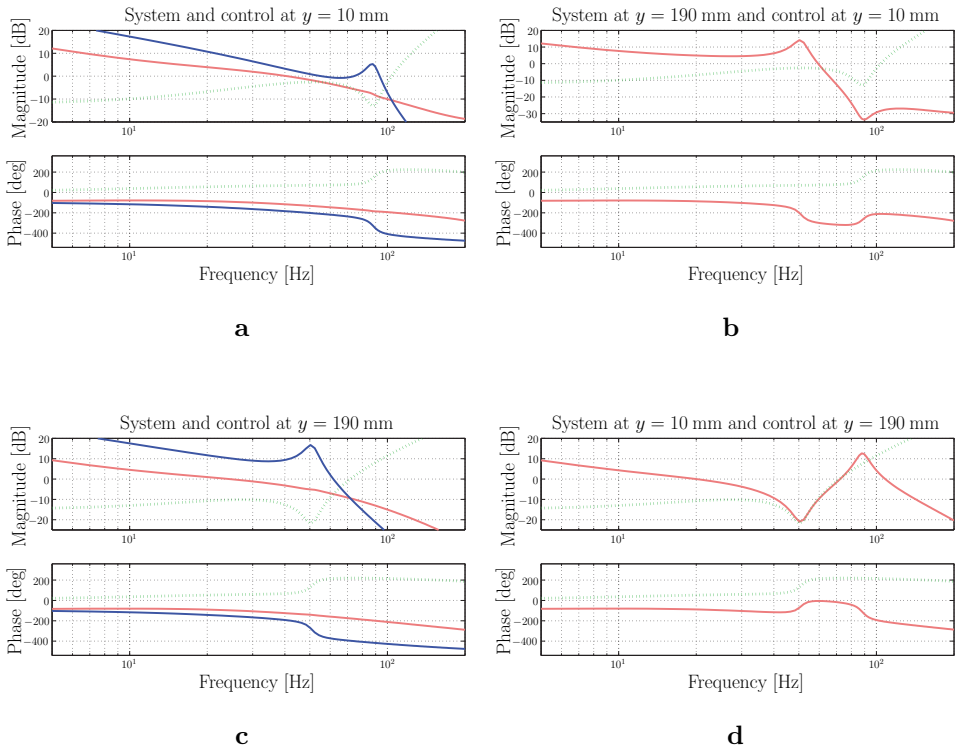

Figure 4.1: This figure shows the problem with the implementation of a notch filter. In **a** and **b**, a controller (green dotted line) with a notch filter is tuned for a system at $y = 10$ mm. The system (dark blue line) and the open loop (light red line) are depicted at two positions: (**a**: $y = 10$ mm and **b**: $y = 190$ mm). The open loop in plot **b** is unstable as the misplaced notch has decreased the phase locally.
In **c** and **d**, a controller (green dotted line) with a notch filter is tuned for a system at $y = 190$ mm. The system (dark blue line) and the open loop (light red line) are depicted at two positions: (**c**: $y = 190$ mm and **d**: $y = 10$ mm). The open loop in **d** is unstable as the misplaced notch has increased the high frequent gain.

This figure shows the problem with the implementation of a notch filter. The open loop in Figure 4.1b is unstable as the misplaced notch has increased the high frequent gain. The open loop in Figure 4.1d is unstable as the misplaced notch has decreased the phase locally. This leads to the conclusion that a controller should be derived that is not too specific for one position, or a controller should be derived that can shift its behaviour as function of the position.

With the classical hydraulic control approach and the $\mathcal{H}_\infty$ control approach, a controller is derived that is not too specific. The LPV controller can change its behaviour as function of the rod position.

4.3 Control lay-out

As Viersma [1990] shows that pressure feedback has a damping effect on the transfer from u_{pos} to y (see Figure 4.2), the control lay-out is chosen as a combination of position and pressure feedback. For all strategies the following control lay-out is chosen (see Figure 4.2).

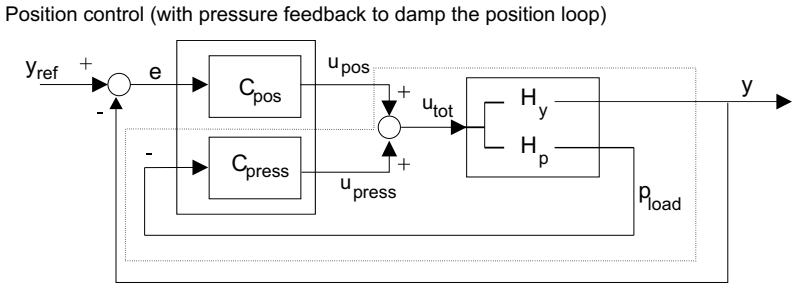

Figure 4.2: The general control layout. Pressure feedback (p_{load}) has a damping effect on the natural frequency. The dotted box depicts $H_{y_{damp}}$. This is a siso system that has u_{pos} as input and y as output. In this siso system the effect of C_{press} is taken into account.

The system has two outputs and one input. The transfer from u_{tot} to y is the position transfer (H_y). The transfer from u_{tot} to p_{load} is the pressure transfer (H_p). The damped position transfer ($H_{y_{damp}}$) is the transfer from u_{pos} to y with the pressure loop closed.

4.4 Classical hydraulic control

Classical hydraulic control is based on linear position feedback. A standard PID controller is designed to achieve position tracking [Franklin et al. 1993,p.337]. The gain and bandwidth of the controller should be conservative enough, to give a stable feedback loop for all rod positions. Additionally, the natural frequency can be damped by means of pressure feedback. Proportional pressure feedback (C_{press}) is added (see Figure 4.2). The position PID controller (C_{pos}), can now be tuned for the damped position transfer ($H_{y_{damp}}$).

In general, proportional pressure feedback is straightforward as the high frequent phase of the pressure loop stays well above -180^{o} (See Figure 2.4 on page 12). In this case, the relatively slow valve lowers the phase of the pressure loop, so the gain of C_{press} is limited by the pressure transfer function. The pressure transfer function (H_p) for a rod position of 10 mm has the highest gain, so C_{press} is limited by H_p at 10 mm. Figure 4.3 shows the position transfer function (H_y) and H_y damped by the maximum pressure feedback ($H_{y_{damp}}$). This figure shows the best way to tune the position PID controller: the phase at the natural frequency lies below 180^{o}. This means the system is so-called 'phase-stabilised' [see Franklin et al. 1993,p.419]. Adding D-action rotates the open loop in the Nyquist plot counter clockwise. This results in cancellation of the phase-stabilisation, so adding D-action is not useful for this system, so the position controller should consist of a gain and possibly an I-action.

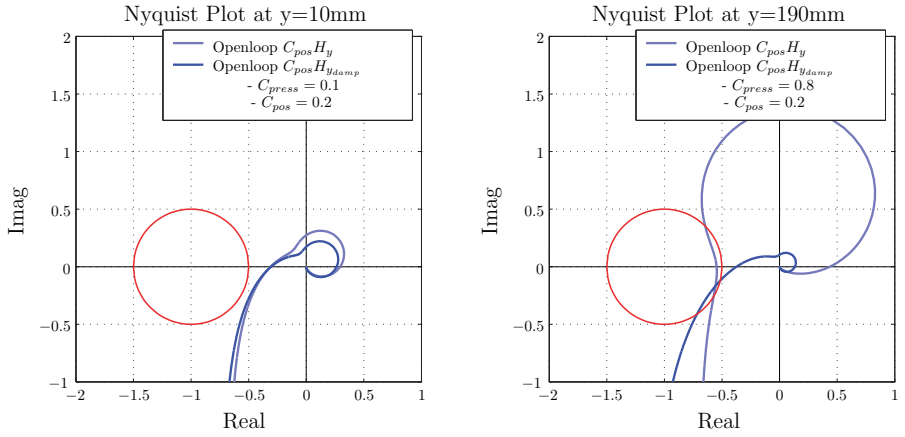

Figure 4.3: Nyquist plot of the open loop system at both the retracted and extended rod positions. The gray line represents the position open loop with a $C_{pos} = 0.2$. The black line represents the position open loop of the system which is damped by means of an extra pressure feedback ($C_{pos} = 0.2$ and $C_{press} = [0.1 \ldots 0.8]$).

4.5 Classical hydraulic control results

Five different controllers are designed with the mimo controller design tool MCDesign [MCDesign 2005]. At rod positions of 10, 50, 100, 190 mm local controllers are designed. A fifth, global, controller is designed to be stable for the whole range without pressure feedback. This later controller is designed to be stable at the most extended rod position as there the system's natural frequency is at its lowest. This controller is also stable for more retracted rod positions where the natural frequency is higher. The global position feedback controller is implemented both with an analog control board and with the discrete dSpace system [dSpace Inc 2005]. The local controller with pressure damping is only implemented with dSpace. Figure 4.4 shows the results for the local controller for a rod position of 50 mm. Figure 4.5 shows the results of the global controller at a rod position of 10 mm.

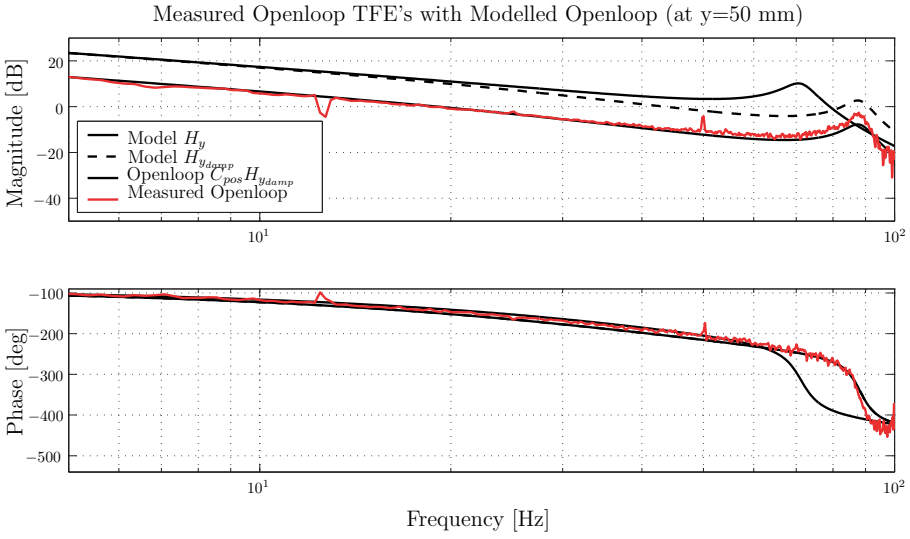

Figure 4.4: The frequency response estimate of the open loop of the local controller for $y = 50$ mm

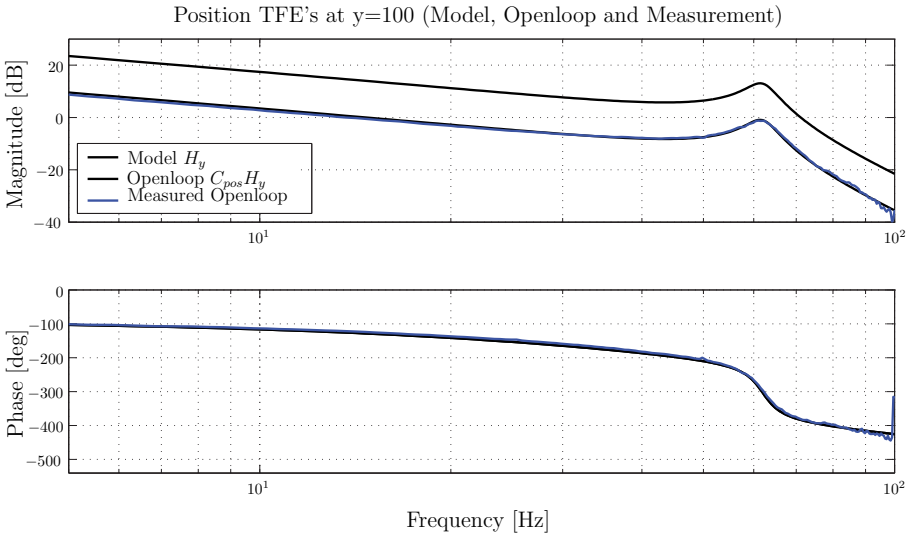

Figure 4.5: Measured open loop of the global controller at $y = 100$ mm, plotted on the modelled open loop.

The controller implemented with dSpace, shows a noisy response, especially at the natural frequency of the system. If the same controller is implemented with the analog control board, the response is more smooth. The vibrations can be caused by amplification of discretisation noise or by aliasing of a high frequent component in the sensor signal. If the discretisation frequency of the discrete controller is changed, the vibration does not change. So the vibration is not caused by an aliasing effect. If the accuracy of the discretisation is increased, the vibration decreases. So the vibration is caused by the amplification of the discretisation noise. This problem is solved by amplifying the position measurement with a gain of five with an analog amplifier. The amplified signal is then discretisised by dSpace. This gives a five times smaller discrete step size and a five times lower noise level. A disadvantage is that the range of the position signal is also decreased. So the system can only be controlled in a range of 40 mm in stead of 200 mm. In appendix D another method is described to increase to dynamic performance of the position sensor.

4.6 Conclusion

In this chapter classical hydraulic controllers are derived. The controller that is stable for the all rod positions consists only of static proportional feedback as the pressure loop for the retracted rod positions is too sensitive to add pressure feedback. The bandwidth reached with the global controller is about 15 Hz. For the more extended rod positions, the pressure loop of the system is less sensitive. Local controllers for those positions can consist of pressure feedback that has a damping effect on the natural frequency of the system. This increases the performance of the system.

The shifting natural frequency of the system prevents the use of a more specific control approach such as notch filters. Furthermore the measurement noise caused by the discretisation introduces a vibration at the natural frequency of the system with digital control.

Chapter 5

$\mathcal{H}_\infty$ control

A more general approach to the control problem is $\mathcal{H}_\infty$ control design. In this approach, certain demands and limitations can be set on performance and robustness. The $\mathcal{H}_\infty$ algorithm searches the controller that meets the demands and limitations. The advantage is that a controller can be tuned that has specific constraints. This is in contrast to the classical control approach in which a controller is tuned for a worst case scenario, hoping it will also be stable for the other positions of the system. In this case the moving natural frequency can be modelled as a model uncertainty. One of the demands set on the $\mathcal{H}_\infty$ controller will be a robustness demand concerning this uncertainty. This way a controller can be derived with a specific robustness for the shifting natural frequency.

The $\mathcal{H}_\infty$ controller is designed to be stable for a rod position range from $100 - 190$ mm.

5.1 Introduction to $\mathcal{H}_\infty$ control

For a theoretical description of $\mathcal{H}_\infty$ control, see literature [Scherer & Weiland 2005]. This thesis focuses on the practical use of $\mathcal{H}_\infty$ control design. $\mathcal{H}_\infty$ control is used as a tuning method to make closed loop properties like the sensitivity (S) or the closed loop behaviour, the complementary sensitivity (T), meet certain criteria. For this purpose, filters are added to the closed loop system (Figure 5.4). This results in a weighted system (M) that is a function of the controller (C) (see eq. 5.1). The $\mathcal{H}_\infty$ algorithm minimises the maximum of all input-output transfers of $M(C)$. This is done by adjusting the controller to minimise the infinity norm (γ) of $M(C)$ (see $\mathcal{H}_\infty$ definition). If $\gamma = 1$, the maximum transfer of all components of eq. 5.1 is less than one. This means for example that $|W_e S V_r| < 1$, so the sensitivity will be $|S| < |(W_e V_r)^{-1}|$. Therefore the chosen shape of W_e and V_r can determine the shape of S. See also Figure 5.1

$\mathcal{H}_\infty$ definition

$$\gamma = \inf_{C \in C_{stab}} \sup_{w \in \mathcal{L}_2} \frac{\|z\|_2}{\|w\|_2} \Longrightarrow C$$

γ is the maximum transfer from any w to any z which will occur for the worst input signal. Minimising γ is achieved by modifying C

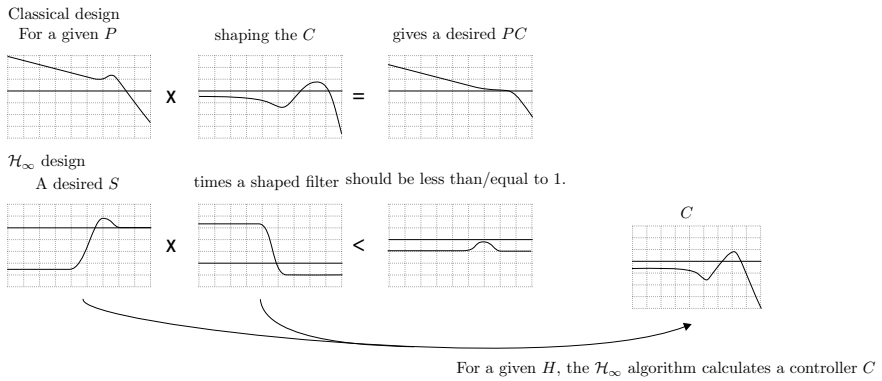

Figure 5.1: **a**: Classical control design: shaping (C) is used to obtain a certain openloop (PC). **b**: By choosing a filter ($Filter$) that is the inverse of the desired sensitivity (S), an $\mathcal{H}_\infty$ algorithm that makes the closed loop transfer 1 automatically find a controller giving a good sensitivity (S).

5.1.1 Mixed sensitivity and four block notation

There is a difference between an $\mathcal{H}_\infty$ layout with one input and two outputs and a $\mathcal{H}_\infty$ lay-out with more inputs and outputs (Figure 5.2). The first lay-out is called a mixed sensitivity problem. The second is a so called four block notation. The mixed sensitivity has two transfers, a sensitivity (S) and a complementary sensitivity (T). The two outputs filters can tune S and T: $|S| < |W_1^{-1}|$ and $|T| < |W_2^{-1}|$. The W_1 filter can be used to enforce the sensitivity below the bandwidth for good tracking and disturbance rejection (this is called performance). The W_2 filter can be used to penalise high frequent dynamics to prevent controller saturation and noise amplification (this is called robustness). The four block notation has more inputs. The transfers from the second input to the outputs are control sensitivity (CS) and process sensitivity (SP). With this lay-out filters can also be designed for CS and SP that give robust performance. This means that the performance demands are also met for the disturbed system.

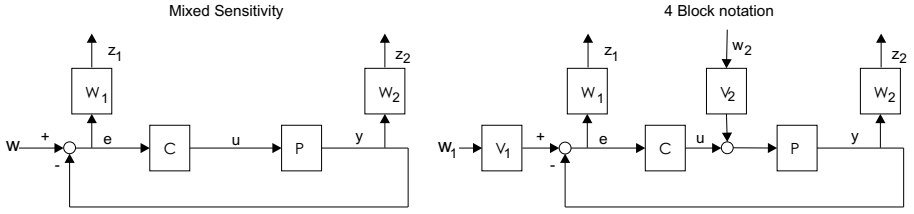

$$z = \begin{bmatrix} W_1 S \\ W_2 T \end{bmatrix} w \qquad z = \begin{bmatrix} W_1 S V_1 & W_2 T V_1 \\ W_1 C S V_2 & W_2 S P V_2 \end{bmatrix} w$$

$$\text{with: } S = (I + PC)^{-1} \quad \textit{and} \quad T = PC(I + PC)^{-1} = PCS$$

Figure 5.2: Mixed sensitivity versus the 4 block notation.

A typical filter tuning example can be given with the mixed sensitivity problem. If the S, T and both inverted filters are plotted in one figure (Figure 5.3), it can be visualised that W_1 shapes S and W_2 shapes T. As $S+T=1$, W_1^{-1} and W_2^{-1} cannot be below the 0 dB line at the same point. Setting both W_1^{-1} and W_2^{-1} below the 0 dB line would lead to a conflict with $S+T=1$ and there would be no solution. So the limiting effect that actuator saturation and plant uncertainty have on T, will automatically limit the S and the performance. In the four block notation a similar effect is present.

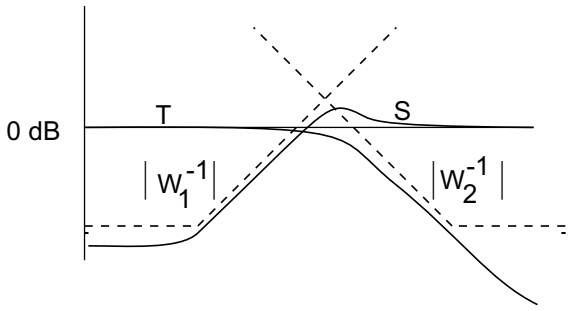

Figure 5.3: Typical mixed sensitivity weights.

5.2 $\mathcal{H}_\infty$ lay-out

The $\mathcal{H}_\infty$ controller that is derived in this chapter should robustly stabilise the system, given the movement of the rod. In addition it should meet performance criteria. The rod movement is limited to a position range of 100 to 190 mm. The change of the natural frequency due to this piston movement is treated as a model uncertainty. The discussed set-up has several properties subjected to certain demands such as: a) tracking, b) limited controller output, c) disturbance rejection. So filters that set limits or demands on control output, noise level, tracking and plant uncertainty have to be added. This results in the lay-out depicted in Figure 5.4. As all these demands must be met for all rod positions the controller must have robust performance. This can be achieved with five filters.

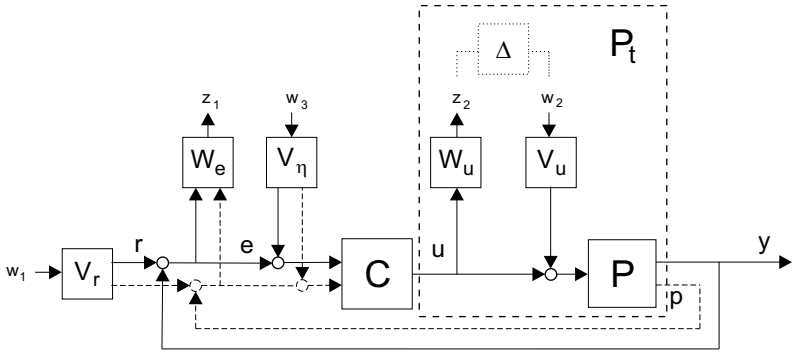

Figure 5.4: General $\mathcal{H}_\infty$ Layout. The solid lines represent the configuration for the siso feedback case. The dashed lines are the connections added to this lay-out for the mimo feedback case. The P_t block is the so called perturbed plant. This is the plant with the multiplicative uncertainty.

$$\begin{bmatrix} z_1 \\ z_2 \end{bmatrix} = \begin{bmatrix} W_eSV_r & W_eSPV_u & W_eTV_\eta \\ W_uCSV_r & W_uTV_u & W_uCSV_\eta \end{bmatrix} \begin{bmatrix} w_1 \\ w_2 \\ w_3 \end{bmatrix} \tag{5.1}$$

Figure 5.4 shows the lay-out chosen for the discussed system. Eq. 5.1 gives the transfer function ($M(C)$) of the system, including the filters and the controller.

5.3 Filter design

The filter tuning can be divided into two parts. First, the filters that represent the physical limits of the system are set. These are the filters representing the model uncertainty, the limitations on

the actuator and the measurement. Second, the filters that are used to tune the controller are tuned.

5.3.1 Actuator limitation

Figure 2.3 shows the actuator acts as a low-pass filter. The actuator cannot actuate the system above approximately 90 Hz. For higher frequencies, the actuator output rapidly decreases for a certain input signal. In the $\mathcal{H}_\infty$ design, high frequent controller output is limited by setting the W_u filter as a low-pass filter with a pole at 90 Hz. The filter is a first order filter to limit the order of the total system. The low frequent gain of the filter is set to one as the actuator has a maximum output of one.

5.3.2 Measurement noise

Time domain position measurements show that the noise on the measured data is approximately 5 times the discrete step size of 0.01 mm plus a bit coloured noise. The noise filter for the position is chosen as a static gain of 0.1. Time domain pressure measurements show that the noise on the measured data is approximately 3 to 4 times the discrete step size of 0.001. The noise filter for the pressure is chosen as a static gain of 0.005.

5.3.3 Plant uncertainty

In the $\mathcal{H}_\infty$ approach, the variations in the plant due to its position dependency, are modelled as an uncertainty. This is done with the 'Delta' block (Δ). Figure 5.4 shows the so called called perturbed plant (P_t). This represents the plant and its uncertainty.

$$P_t = (I + V_u \Delta W_u)P \tag{5.2}$$

With $P_t = (I + V_u \Delta W_u)P$ and Δ ($\|\Delta\|_\infty < 1$) as the scaled multiplicative uncertainty, it follows from the small gain threorem that the closed loop system is robustly stable if the transfer function from w_2 to z_2 has a gain (∞-norm) which less than one [Damen & Weiland 2002,p.77].

The filter W_u is already tuned. The V_u filter is used to make $P_t = (I + W_u \Delta V_u)P$. If P_i is one of the manifestations of P for a certain rod position y, then $|P_t|$ should be greater than $|P_i|$ for all i. This means that $|(I + W_u \Delta V_u)P| \geq |P_i|$ and if $\|\Delta\|_\infty = 1$ this leads to eq 5.3

$$|W_u V_u| \geq \frac{|P_i - P|}{|P|} \qquad ,\forall i \tag{5.3}$$

A plot of $\frac{|P_i - P|}{|P|}$ can be made for different i. Figure 5.5 shows this plot for the P_i of the minimum and the maximum rod positions. The overlaying curve (δP)is greater than P_i for all i. This δP is used as $W_u V_u$. As W_u is already tuned, V_u is calculated by $\delta P W_u^{-1}$.

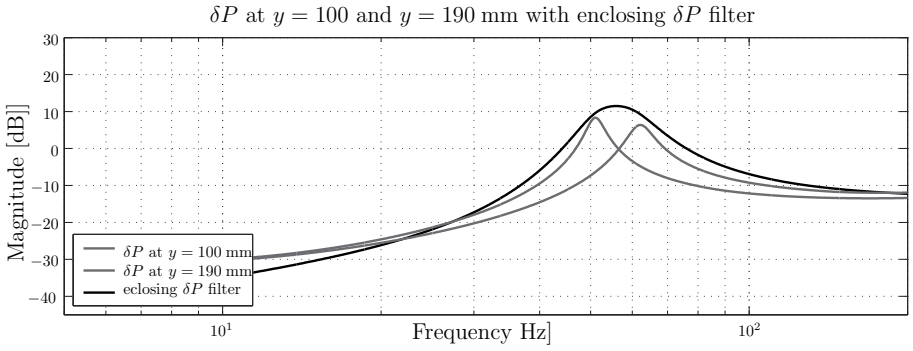

Figure 5.5: δP at $y = 100$ and $y = 190$ mm with enclosing W_u V_u filter

The pressure transfer function of the plant has the same uncertainty as the position transfer function as the relationship between pressure and position is independent of the position. So the same δP can be used for the pressure transfer function. The advantage is that in the mimo case, the same filters can be used to model the plant uncertainty.

5.3.4 W_e and V_r filter tuning

The filters W_e and V_r are used to tune the controller performance. Similar to the described method for the mixed sensitivity problem (see 5.1.1), the W_u V_u and V_η filter put a limit on T. This means that they automatically put a limit on S as well.

The starting point for the filter tuning is an initial choice for W_e and V_r. The reference modelled in V_r is chosen by comparing the physical maximum of the system. The system can move over ± 45 mm with a maximum speed of $\frac{q_N}{A} = 300$ mm s^{-1} and a maximum acceleration of $\frac{F}{m} = \frac{p_s A}{m} = 5720$ mm s^{-2}. This results in the following reference:

The error filter W_e is chosen to set the error weighting as twice the size of the measurement noise. Theoretically, the error cannot be less than the accuracy. In this case the error should be less than twice the measurement noise. So the W_e filter has a low frequent gain of 5, which is twice the inverse of the V_η filter. The W_e filter is chosen as a 2^{nd} order low pass filter. This means that the high frequent errors are not weighted. The pole of this filter is placed at 34 Hz. This gives the filter the same 0 dB crossing as the W_e filter.

5.4 Position feedback

Both a siso $\mathcal{H}_\infty$ controller with only position feedback and a mimo $\mathcal{H}_\infty$ controller with both pressure and position feedback are derived. This chapter describes the filter tuning and implementation of the siso controller. The controller is derived with the Matlab algorithm `hinfsyn.m`. This algorithm minimises the infinity norm of $M(C)$ (see eq. 5.1) by adjusting C. The output of the algorithm is the found controller and the infinity norm (γ). For the chosen filters, the algorithm cannot find a controller that makes $\gamma < 1$. The demands on the system are too high, so a new choice has to be made for the W_e and V_r filters.

If $\|M(C)\|_\infty < \gamma$, then all elements of $M(C)$ are smaller than γ. Just as explained in section 5.1.1 and Figure 5.3, this means that $|S| < |\frac{\gamma}{W_e V_r}|$, $|SP| < |\frac{\gamma}{W_e V_u}|$ etcetera. So a plot can be made of S, T, SP and CS, with the inverse of the corresponding filters. This plot shows which filters limit the algorithm in finding a controller that decreases γ below one. Figure 5.6 shows this plot for the controller derived with the current filters. The demands on the performance (W_e and V_r filter) are to high for the limits set by controller output (W_u filter), by the plant uncertainty (V_u

filter) and by the noise level (V_η filter).

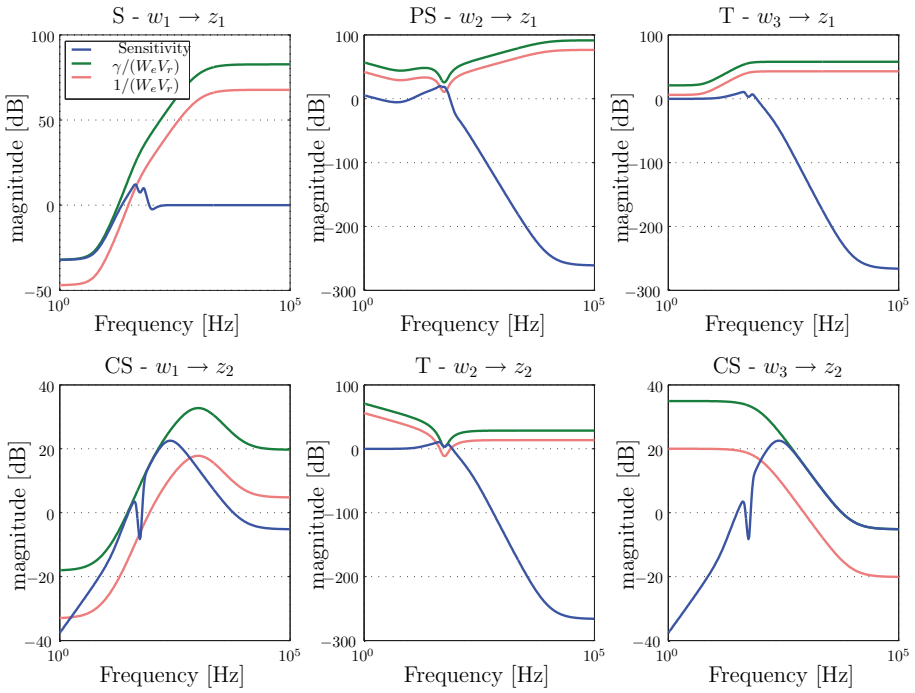

Figure 5.6: The closed loop properties (S, T, SP, CS) shaped by the inverse of the filters ($\frac{\gamma}{W_e V_r}$ etcetera.) This figure shows the situation with the initial filters. The light lines are the shape demands set by the filters. The dark lines depicts the achieved situation.

5.4.1 Position feedback filter tuning

To find an appropriate controller, the demands on the performance are decreased, so a new choice is made for the W_e and V_r filter. With this choice, the demands on the system in V_r should be lower than what is achievable with the system. This is calculated by taking the product of the allowed controller effort and the plant gain ($W_u^{-1}P$). This means that $W_u V_r P^{-1} < 1$.

The V_r filter is replaced by a 2^{nd} order filter. The gain of the V_r filter is decreased and the pole of both the W_e and the V_r filter are decreased. With this new choice, another controller is calculated that indeed leads to a solution. Now the gain and bandwidth of the V_r filter is increased step by step until the $\mathcal{H}_\infty$ algorithm cannot find a controller anymore with $\gamma < 1$. This results in a V_r filter with a low frequent gain of 20 dB and a pole at 3 Hz. The W_e filter has a low frequent gain of 5 dB and a pole at 6 Hz. The solution found with these filters is depicted in Figure 5.7.

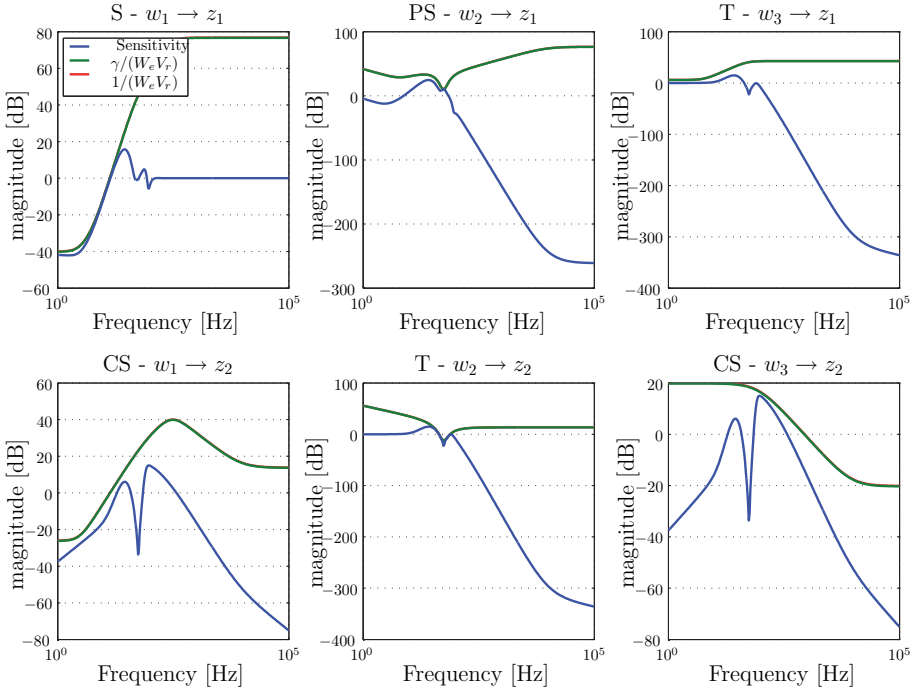

Figure 5.7: The closed loop properties (S, T, SP, CS) shaped by the inverse of the filters ($\frac{\gamma}{W_e V_r}$ etcetera.) This figure shows the first situation with $\gamma < 1$.

This is still not a good solution for the problem, as the sensitivity has a peak that is too high. This peak leads to an overshoot in the time domain. This peak is caused by the choice for W_e and V_r. These filters have no high-frequent component so they do not suppress high-frequent dynamics. The overshoot can be suppressed by adding a high frequent component to the W_e and V_r filters (See Figure 5.8b). Increasing the V_r filter will also increases the demands in the region where the peak in the plant uncertainty disables any demands on tracking. So the sensitivity overshoot should be suppressed by introducing a small bump in the V_r filter (Figure 5.8c).

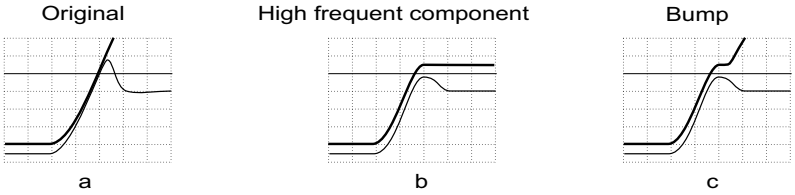

Figure 5.8: Sensitivity overshoot suppression.

To enable a lower high-frequent sensitivity, the low-frequent sensitivity should be somewhat higher. So the low frequent gain of the filters is decreased slightly. After suppressing the sensitivity, the bandwidth of W_e and V_r is further increased in order to increase the performance of the controller. This leads to W_e and V_r filters with poles at 12 Hz. The V_r filter has a low frequent gain of 15 dB and the W_e filter has a low frequent gain of 5 dB. The solution found with these filters is depicted in Figure 5.9.

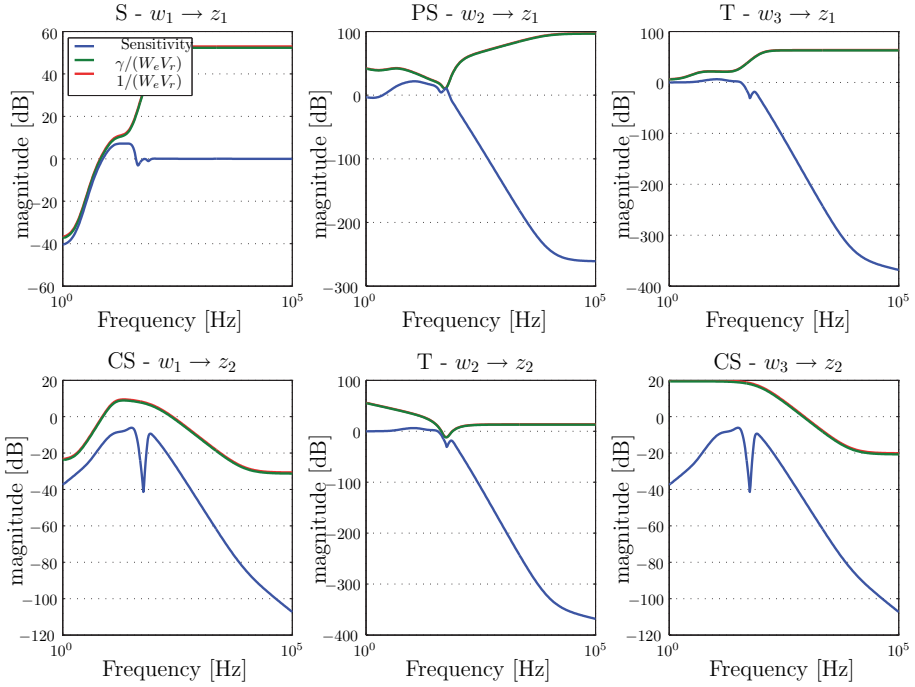

Figure 5.9: The closed loop properties (S, T, SP, CS) shaped by the inverse of the filters ($\frac{\gamma}{W_e V_r}$ etcetera.) This figure shows the situation with the final filters.

5.4.2 Position feedback results

The controller derived in the previous section is depicted in Figure 5.10. The controller has a dip around the average natural frequency. As the system's phase shifts over 180^{o} at the natural frequency and this frequency is uncertain, the plant uncertainty at this frequency is equal to the magnitude of the system. This makes the δP filter greater than 0 dB around the natural frequency: so the magnitude of the open loop around this frequency has to be less than 0 dB which results in this dip. Figure 5.10 shows that the dip is wide and deep enough to ensure that the magnitude of the open loop stays low enough for the range of natural frequencies.

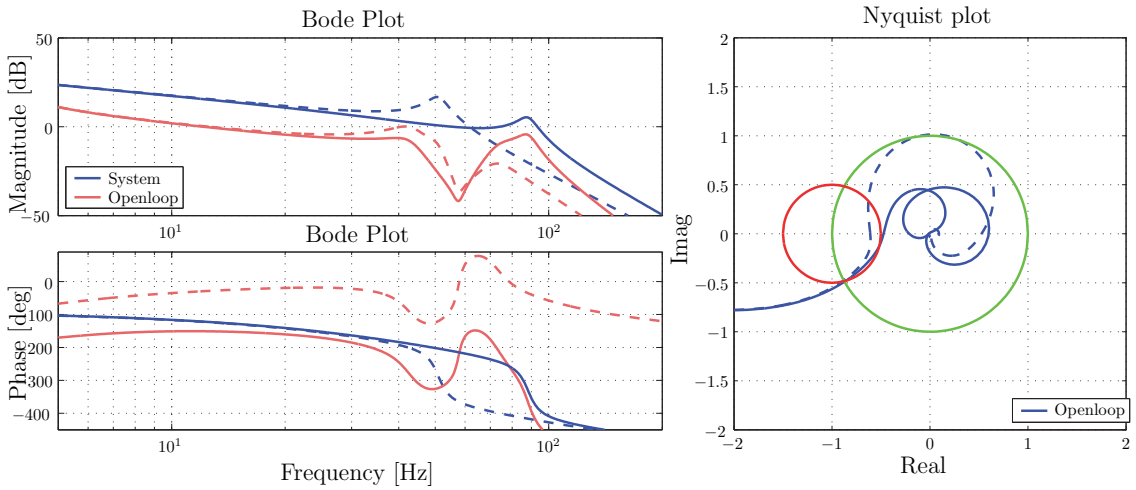

Figure 5.10: The $\mathcal{H}_\infty$ controller with the system and open loop at 100 mm (solid lines) and 190 mm (dashed lines).

The controller furthermore consists of a gain, some I action, and some D-action. This results in a controller with a bandwidth of approximately 10 Hz. So the controller is formed from a PID controller with a dip around the natural frequency of the system to cope with the shifting natural frequency. This solution for dealing with the shifting natural frequency is not better than the classical controller approach as it does not leads to a higher bandwidth. This leads to the conclusion that in this case, the $\mathcal{H}_\infty$ approach is not better than the classical approach.

5.4.3 Position feedback implementation

Before implementation, some controller reduction is performed. From both controllers the balanced realisation is calculated. The least significant states of the resulting balanced realisations are deleted. This is done in order to reduce the complexity of the controllers. Furthermore, a discretisation is applied to the controllers using a 1^{st}-order-hold algorithm. This transformation also deletes all high frequent control action resulting from the used $\mathcal{H}_\infty$ algorithm (see Figure 5.10).

The position controller works as designed (see Figure 5.11). The performance is comparable with the designed performance. The system only has a vibration at the natural frequency that is probably caused by amplification of discretisation noise (see section 4.5).

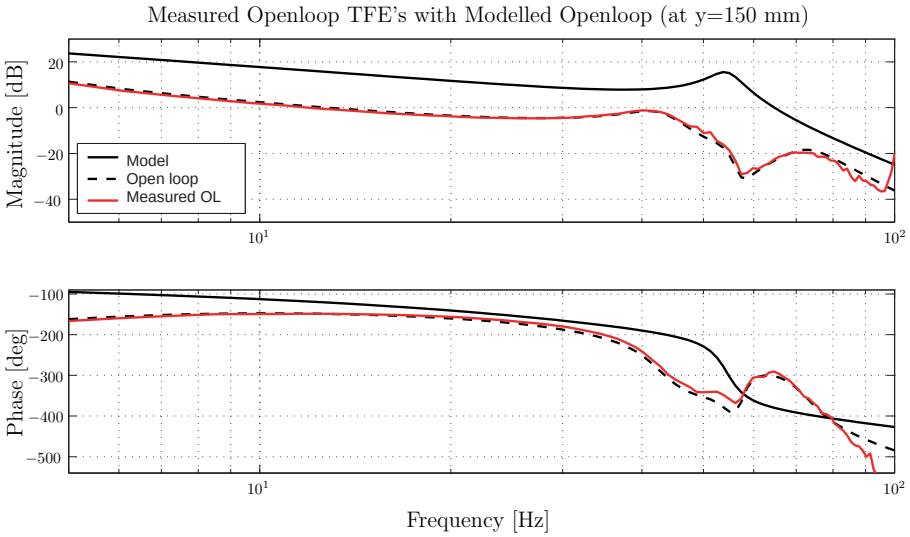

Figure 5.11: $\mathcal{H}_\infty$ controller at 150mm

5.5 Position and pressure feedback

In the classical hydraulic approach, pressure feedback damps the open loop transfer of the position loop. Therefore, an $\mathcal{H}_\infty$ controller with pressure feedback is also designed. For the controller with pressure feedback, the same lay-out as depicted in Figure 5.4 is used. The difference is that now V_r, V_η and W_e are 2×2 diagonal filters. This means a second reference is introduced. As the pressure and position cannot be controlled independently and no pressure reference exists, it is not correct to add a second reference. The error made by introducing a 2^{nd} reference is minimised by setting V_{r_2} and W_{e_2} very low. The advantage of this lay-out is that filter tuning remains similar to the position feedback case. Vn_{η_2} is set at 5 times the sample frequency. This results in a V_{η_2} filter with a static gain of 0.005. The V_u and W_u filter are chosen the same as in the siso case.

5.5.1 Position and pressure feedback filter tuning

The filter tuning for the position and pressure feedback case is similar to the position feedback case. The difference is that $M(C)$ (eq. 5.1) has become greater. As the W_e V_r and V_η filters are 2×2 filters, $M(C)$ becomes a 3×5 system (see eq. 5.4). As W_e V_r and V_η are diagonal filters, 4 elements become zero. As V_{r_2} and W_{e_2} are very low, 5 more elements are very low. So compared with the siso case, only one more filter can limit the closed loop properties of the mimo system. This is the filter that defines the noise level on the pressure measurement. As this noise level is low compared with the noise level on the position measurement, this is also not limiting for the control design. So for the filter tuning the same figures are used as shown in the previous section.

$$\left[\begin{array}{c} z_{1_1} \\ \hline z_{1_2} \\ \hline z_2 \end{array}\right] = \left[\begin{array}{cc|c|cc} W_{e_1}S_{1,1}V_{r_1} & 0 & W_{e_1}SP_1V_u & W_{e_1}T_{1,1}V_{\eta_1} & 0 \\ 0 & \sim 0 & \sim 0 & 0 & \sim 0 \\ \hline W_uCS_1V_{r_1} & \sim 0 & W_uTV_u & W_uCS_1V_{\eta_1} & W_uCS_2V_{\eta_2} \end{array}\right] \left[\begin{array}{c} w_{1_1} \\ w_{1_2} \\ \hline w_2 \\ \hline w_{3_1} \\ w_{3_2} \end{array}\right] \quad (5.4)$$

The filters are initially set as the filters used in the position feedback case. The bandwidth of the V_r and W_e filter is increased. The bump in the filters is shifted separately to give enough sensitivity

suppression in order to keep the sensitivity below 6 dB. This results in the filters depicted in Figure 5.12.

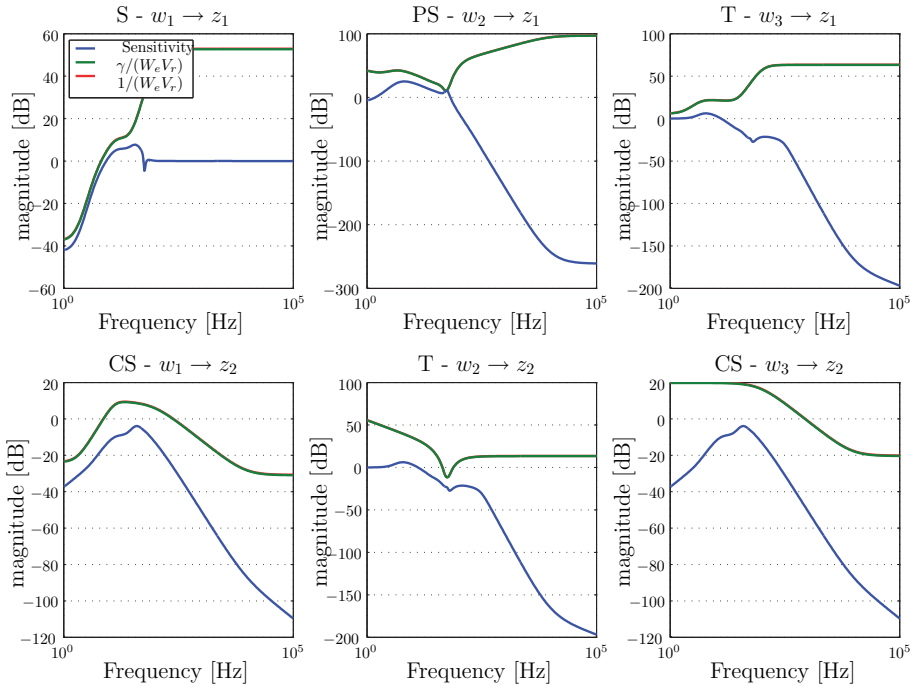

Figure 5.12: The closed loop properties (S, T, SP, CS) are shaped by the inverse of the filters ($\frac{\gamma}{W_e V_r}$ etcetera.) This figure shows the situation with the final filters for the position and pressure feedback.

5.5.2 Position and pressure feedback results

The controller found by the algorithm is depicted in Figure 5.13. The controller is analysed using the classical hydraulic control approach. The pressure feedback loop is considered to damp the position transfer of the system. The position feedback loop is considered to act at the damped position transfer ($H_{y_{damp}}$) (see also Figure 4.2. The pressure feedback loop is unstable (see Figure 5.13a till 5.13c) and gives an approximately static positive pressure feedback. Figure 5.13d and 5.13e show that this indeed decreases the difference in $H_{y_{damp}}$ for the different rod positions. It also makes $H_{y_{damp}}$ unstable. To stabilise this transfer, the open loop of the position feedback has to encircle the -1-point in the Nyquist plot (see Figure 5.13f) . This results in a position open loop with a slightly higher bandwidth than the siso $\mathcal{H}_\infty$ open loop of section 5.4.

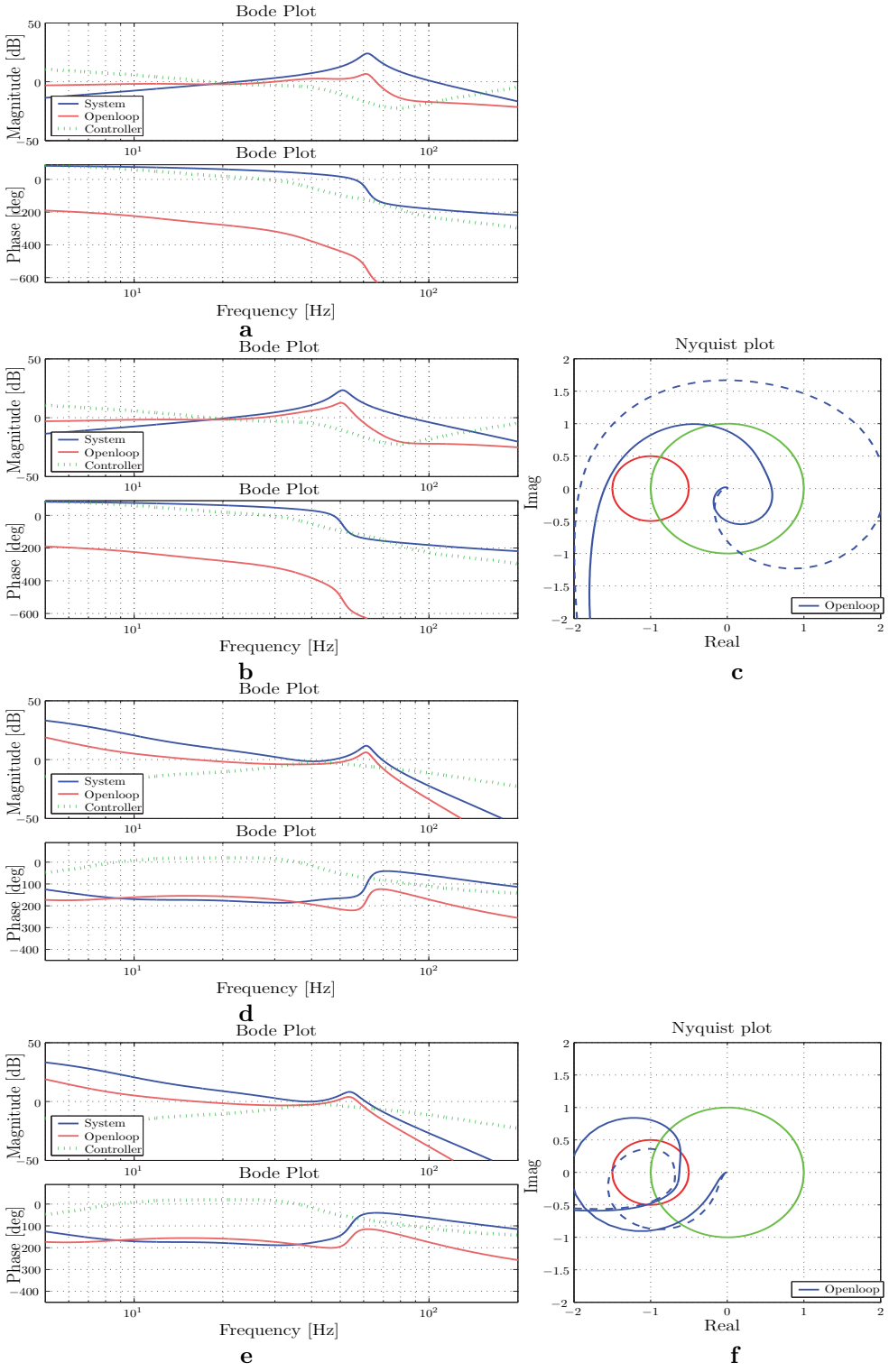

Figure 5.13: The position and pressure feedback $\mathcal{H}_\infty$ controller.
a depicts the pressure open loop. The dark blue line is the pressure transfer function. The green dotted line is the pressure controller (C_{press}). The light red line is the corresponding open loop. **c** gives Nyquist plots for the open loops from **a** and **b** . The solid line is the open loop for $y = 100\,\text{mm}$, the dotted line for $y = 190\,\text{mm}$. Plot **d**, **e** and **f** depicts the similar transfers for the position open loop. The position transfer function is $H_{y_{damp}}$ (The position transfer function damped by the pressure loop).

The natural frequency is not damped as was expected nor is the bandwidth increased significantly. The problem is that, although the pressure feedback can damp the system, it cannot damp the plant uncertainty filters. The uncertainty, modelled in the V_u and W_u filters, is not decreased if pressure feedback is added. Only a minor improvement is gained with the pressure feedback. The price is an unstable pressure loop that can cause problems in implementation. This leads to the conclusion that this $\mathcal{H}_\infty$ controller is also not better than the previous $\mathcal{H}_\infty$ controller. It is also not better than the classical controller.

5.5.3 Position feedback implementation

The implementation of the pressure and position controller was not successful. The controlled system is unstable. The system winds up at approximately 6 Hz. This is about the natural frequency of the supporting table. Due to the unstable pressure loop, the stability of this controller is too sensitive for low frequent model errors. The problem can be solved by better modelling. However, as this $\mathcal{H}_\infty$ approach is not very promising, this is not undertaken.

5.6 Conclusion

In this chapter two $\mathcal{H}_\infty$controllers are derived: a siso position controller and a mimo pressure and position controller. The siso $\mathcal{H}_\infty$ controller has a bandwidth of approximately 10 Hz. This is comparable to the bandwidth of the classical hydraulic controller. This means that, although the $\mathcal{H}_\infty$ algorithm gives another controller then the classical hydraulic controller, it cannot find a better control approach.

The $\mathcal{H}_\infty$ approach could probably have found a better control approach if the plant uncertainty around the natural frequency had been smaller. In the case discussed in this thesis the plant uncertainty is higher then one, which suppresses all controller action. If the range of natural frequencies is that small that the uncertainty drops below one, the $\mathcal{H}_\infty$ control approach probably can find a controller that gives a bandwidth higher than the natural frequency.

The $\mathcal{H}_\infty$ controller consisting of both pressure and position feedback consists of an unstable pressure loop that makes the position loop less position dependent. This results in a slightly higher bandwidth. However, this controller could not be implemented since tests shows that the controller is unstable. This is probably caused by the unstable pressure loop that is sensitive to model errors.

Chapter 6

LPV control

In the previously reported strategies, the moving complex-pole pair of the system limits the control design. So finding a control strategy that can adapt to this non-linearity is a logical choice. Linear parameter varying control (LPV control) is a variation of the described $\mathcal{H}_\infty$ approach. The difference is that, in the LPV algorithm the plant and controller can be dependent on the rod position. The $\mathcal{H}_\infty$ algorithm is replaced with an algorithm that finds a robust controller that can vary in the same parameter θ as the model of the LPV system. The expectation is that the LPV controller can apply more specific control actions, such as a notch filter, to increase the bandwidth as depicted in Figure 4.1.

6.1 Introduction to LPV control

The LPV controller design is similar to the $\mathcal{H}_\infty$ controller design. The same filters and tuning methods are used. The difference is that this controller depends on the same parameter θ as the model. The advantage is that the controller can vary for different positions. Both the plant (P) and the controller (C) are linear depending on θ and θ is a nonlinear function of the position (see eq. 3.4 on page 16). The shifting natural frequency can be modelled with this LPV model. This decreases the plant uncertainty. As a result of this, the demands on the controller can be increased, which should lead to a stiffer controller with a higher bandwidth.

Current LPV algorithms make the calculated controller robust for dynamic behaviour of θ. The hydraulic cylinder however can only move relatively slowly over considerable distances. So the LPV algorithm should calculate a controller that is robust for limited dynamic behaviour of θ, otherwise the calculated controller will be too conservative. However, the used algorithms cannot discount the limited dynamic behaviour of θ. This is why controllers derived with the LPV algorithm will be too conservative.

LPV definition

$$\gamma_{LPV} = \sup_{\theta \in \mathcal{P}} \inf_{C \in C_{stab}} \sup_{w \in \mathcal{L}_2} \frac{\|z_\theta\|_2}{\|w\|_2} \Longrightarrow C(\theta)$$

γ is the maximum transfer from any w to any z for the worst input signal and for the worst $\theta(t)$. versus the $\mathcal{H}_\infty$ definition where γ is the maximum transfer from any w to any z for the worst input signal.:

$$\gamma_{\mathcal{H}_\infty} = \inf_{C \in C_{stab}} \sup_{u \in \mathcal{L}_2} \frac{\|z\|_2}{\|w\|_2} \Longrightarrow C$$

Both the advantage of the adaptability of the controller and the disadvantage of the increased conservativeness, are observed in this chapter. First, a set of $\mathcal{H}_\infty$ controllers is tuned for different rod positions. These controllers can be much stiffer than the previous $\mathcal{H}_\infty$ controllers as the plant uncertainty is decreased. As the LPV controller will be tuned with one set of filters, all local $\mathcal{H}_\infty$ controllers are also tuned with the same filters. The difference between the $\mathcal{H}_\infty$ controllers and the LPV controller is only the robustness for infinitively fast changes in θ.

Next, the same filters are used to calculate one LPV controller. As this controller has to be more conservative, the controller performance will probably have to be decreased. So the filters will have to be tuned again for the LPV controller.

6.2 LPV position feedback

For the LPV control approach, only a position feedback case is examined. The LPV algorithm should be able to cope with the shifting natural frequency, so the pressure feedback is not required.

6.2.1 LPV filter tuning

First the new plant uncertainty is derived. This is done in a similar way, as described for the $\mathcal{H}_\infty$ approach in section 5.3.3. The δP is derived with the same formula: (eq. 6.1)

$$|W_u V_u| \geq \frac{|P_i - P|}{|P|} \qquad ,\forall i \tag{6.1}$$

For the $\mathcal{H}_\infty$ approach, P is the nominal plant and P_i are the plant models at different positions. For the LPV approach $P_i - P$ is the difference between the transfer function of the LPV model for a certain position and the measured transfer function for the same position. The plant uncertainty is modelled with the filters W_u and V_u. The W_u filter stays the same as for the $\mathcal{H}_\infty$ approach, as it also limits the controller output. The V_u filter now becomes: $\delta P/W_u$. With δP as the LPV plant uncertainty.

Secondly, the set of local $\mathcal{H}_\infty$ controllers is tuned in similar way to those of section 5.1. The bandwidth of the W_e and V_r filter can be increased, as the V_u filter is decreased. This leads to the filters depicted in Figure 6.1.

These filters are used to derive an LPV controller with the Matlab function `hinfgs.m`. The LPV algorithm cannot find a controller with $\gamma < 1$ for the same filters. This was expected as the controller has to be more conservative to be robust for the dynamics in θ. If the performance demands on the controller are decreased to the situation as in Figure 6.2, γ stays higher than one, but the robustness for the plant uncertainty is met. As explained in section 5.3.3, robustness for plant uncertainty is achieved if the weighted complementary sensitivity is less than one. This demand is met in the situation depicted in Figure 6.2. This LPV controller is compared with the $\mathcal{H}_\infty$ controllers.

6.3 LPV results

Of the set of local $\mathcal{H}_\infty$ controllers, two controllers are depicted in Figure 6.3. As expected, the local $\mathcal{H}_\infty$ controllers shift the natural frequency to higher frequencies by applying a notch filter. The controllers for the different positions also have notch filters placed at different frequencies. Furthermore the controller consists of a gain, some I action and some D-action. Due to the decreased, but still present, plant uncertainty, the control action is limited around the natural frequency of the system. In this case the control action is only limited, but not fully suppressed as is the case for the global $\mathcal{H}_\infty$ controllers. So the $\mathcal{H}_\infty$ controllers are able to increase the bandwidth

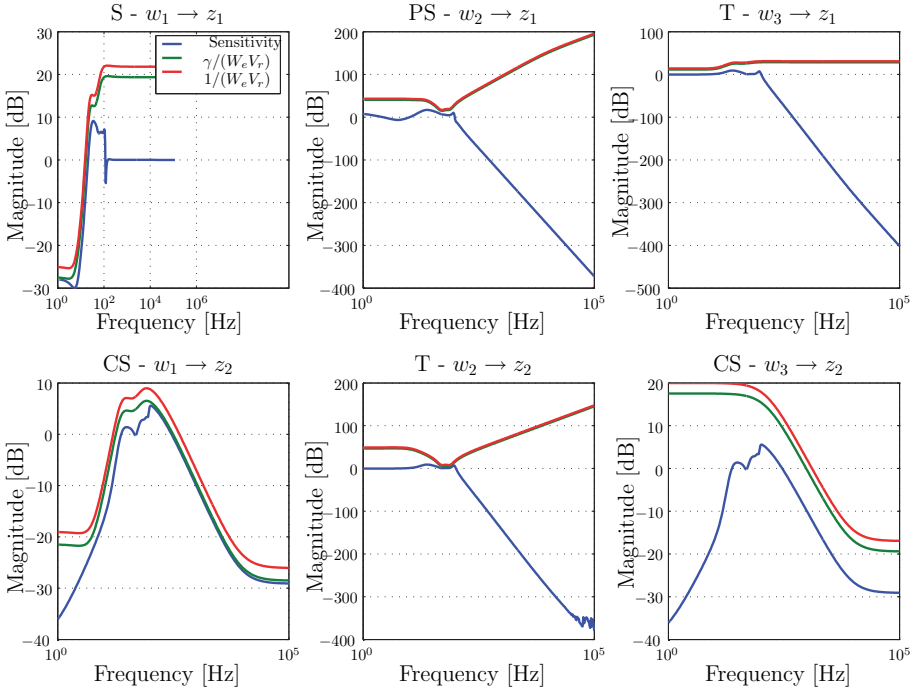

Figure 6.1: Filters tuned for the local $\mathcal{H}_\infty$ controllers. The depicted S, T, CS and SP are for the system at $y = 0$ mm. The same filters are used to calculate controllers at other positions.

to 25 Hz. This is a significant improvement compared with the classical controller and the global $\mathcal{H}_\infty$ controller.

The LPV controller derived with the filters tuned for the LPV controller is depicted in Figure 6.4. This controller is indeed much more conservative than the local $\mathcal{H}_\infty$controllers. The controller is damped a great deal more and does not have the shifting notch filter. So the bandwidth, increased by the local $\mathcal{H}_\infty$ controller, is again decreased to approximately 10 Hz. A a result of this, the LPV controller performance is approximately the same as the $\mathcal{H}_\infty$ controller performance from the previous section (see Figure 5.10).

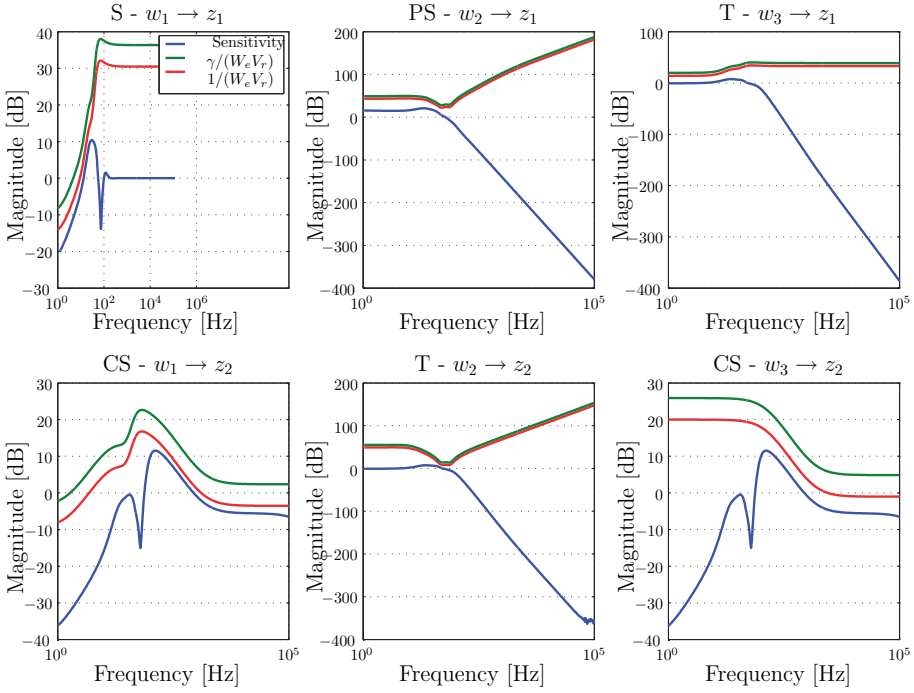

Figure 6.2: Filters for LPV controller.

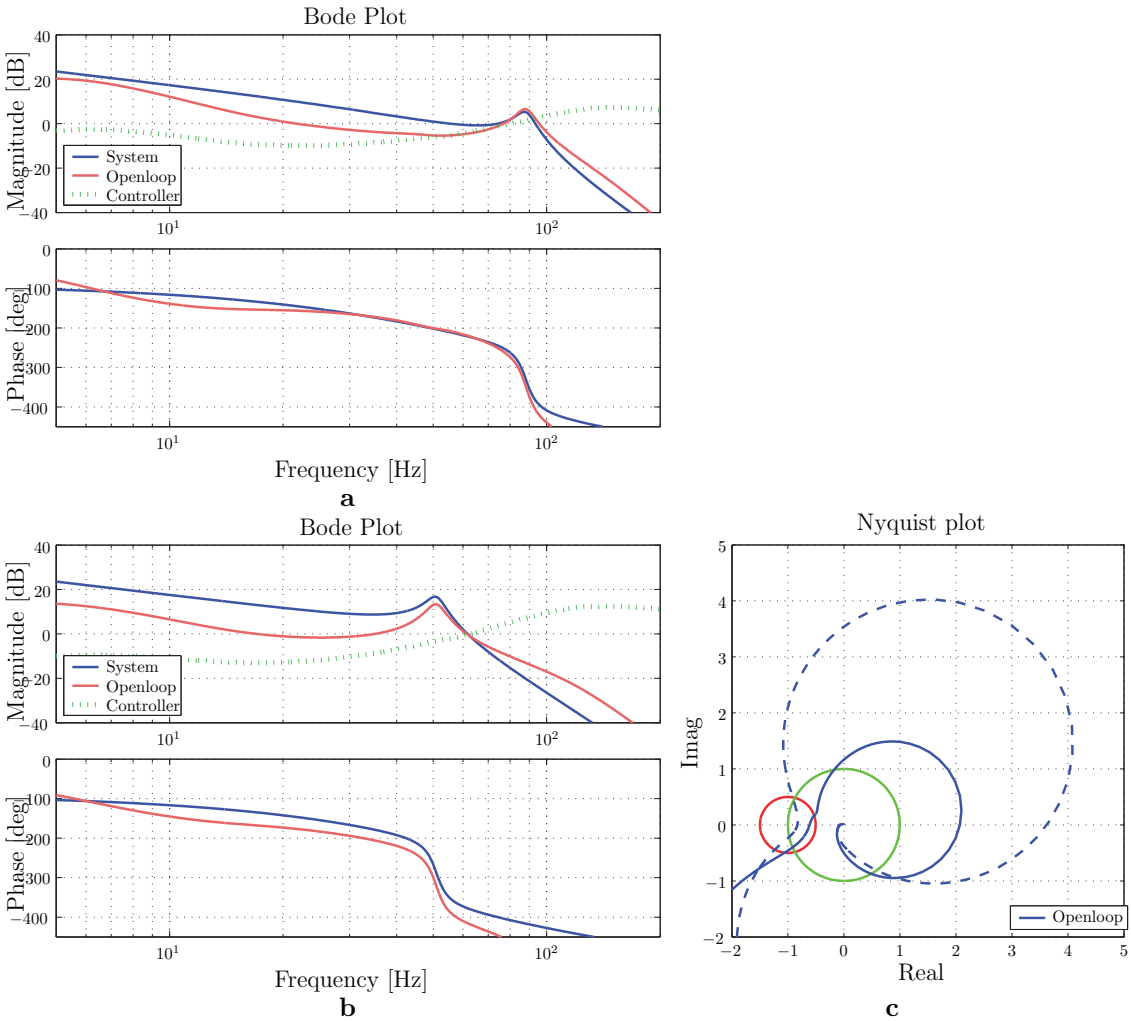

Figure 6.4: The LPV controller with the system and open loop at **a**: 10 mm and **b**: 190 mm. **c** gives both open loops in a Nyquist plot. The dotted line as at 190 mm and the solid lines is at 10 mm.

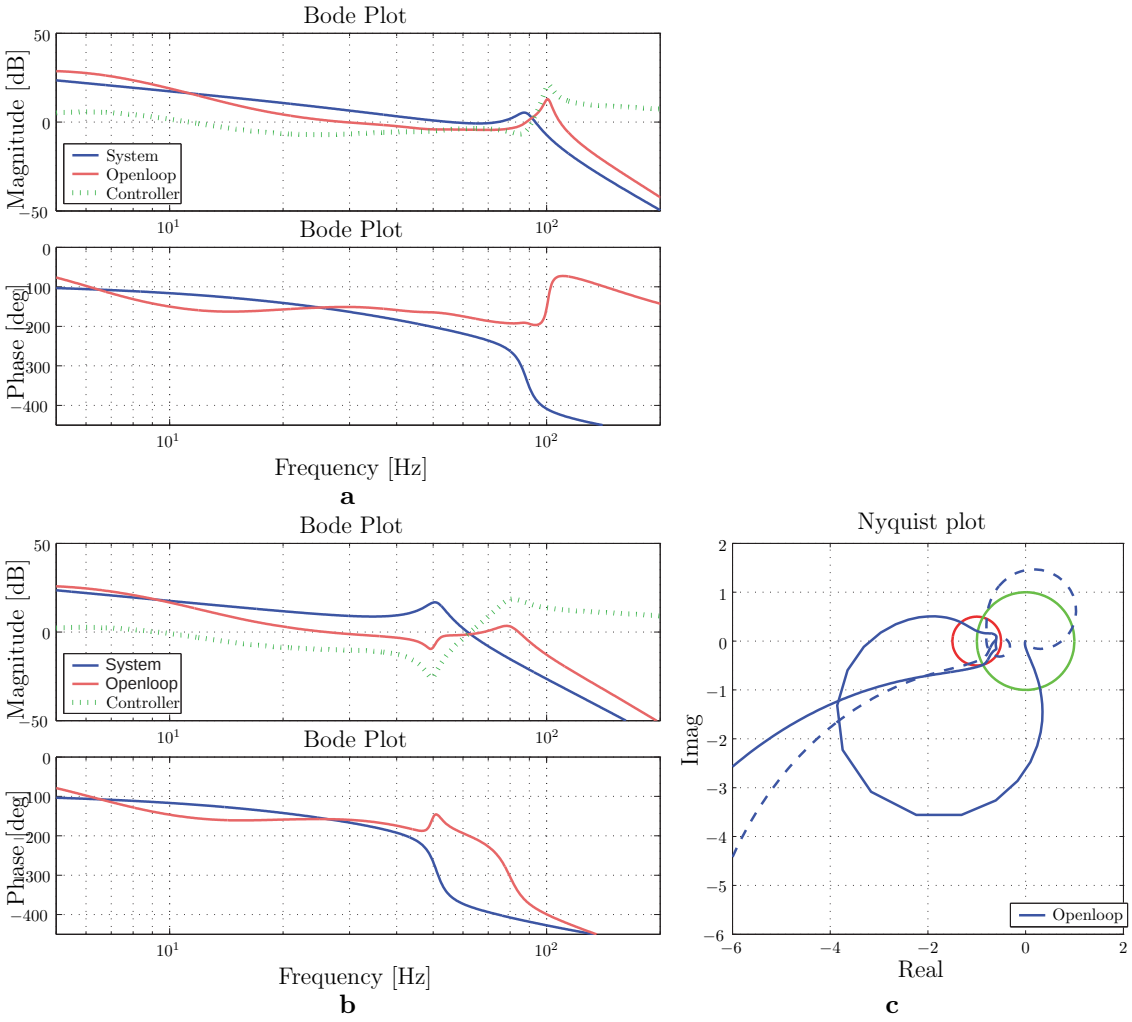

Figure 6.3: Two local $\mathcal{H}_\infty$ controllers with the system and open loop at **a:** 10 mm and **b:** 190 mm. **c** gives both open loops in a Nyquist plot. The dotted line as at 190 mm and the solid lines is at 10 mm.

This leads to the conclusion that the concept of the LPV controller works as expected, but that the algorithm is too conservative to include the required notch filter. Algorithms with adjustable weights on the speed of θ are less conservative and should be able to come up with results comparable with separately tuned $\mathcal{H}_\infty$ controllers. These algorithms are not yet available in Matlab.

6.4 Discretisation

The LPV controller is tested in practice. Before implementing the LPV controller, undesired high frequent dynamics should are deleted. Furthermore, the LPV controller must be transferred to the discrete domain. Common 1^{st}-order hold algorithms are, however, are not sufficient in this case. The LPV controller is built-up out of two state space systems (see eq. 6.2 and eq. 6.3). For a certain value of θ, the corresponding state space system is derived by a linear interpolation of the system matrices. Therefore, transformations applied to the system states are applied on both state space systems. Furthermore, no nonlinear transformations can be made. Common discretisation algorithms use nonlinear algorithms.

Apkarian [1997] makes some suggestions and Trangbæk [2001] derives a method on the discretisation of LPV controllers. One of the main problems with these methods is that the controller has to be discretised at each sample, which is not necessarily feasible in real-time. So another transformation to the discrete domain has to be found.

The LPV controller is written in the polytopic form (with $\theta_2 = 1 - \theta_1$):

$$\begin{aligned} \dot{\mathbf{x}} &= (\theta A_1 + \theta_2 A_2) \cdot \mathbf{x} + (\theta B_1 + \theta_2 B_2) \cdot \mathbf{u} \\ \dot{\mathbf{y}} &= (\theta C_1 + \theta_2 C_2) \cdot \mathbf{x} + (\theta D_1 + \theta_2 D_2) \cdot \mathbf{u} \end{aligned} \tag{6.2}$$

This can be rewritten in in the following matrix-form:

$$\begin{bmatrix} \dot{x_1} \\ y_1 \end{bmatrix} = \begin{bmatrix} A_1 & B_1 \\ C_1 & D_1 \end{bmatrix} \begin{bmatrix} x \\ u \end{bmatrix} \qquad \begin{bmatrix} \dot{x_2} \\ y_2 \end{bmatrix} = \begin{bmatrix} A_2 & B_2 \\ C_2 & D_2 \end{bmatrix} \begin{bmatrix} x \\ u \end{bmatrix} \tag{6.3}$$

With the integration from $\dot{x_1}$ and $\dot{x_2}$ to x defined as: $x = \int \theta_1 \dot{x_1} + \theta_2 \dot{x_2}\, dt$, and the general output defined as: $y = \theta_1 y_1 + \theta_2 y_2$.

These state space systems cannot be transferred to a discrete time system using a zero order hold algorithm as this is a nonlinear transformation of the states. The trick to make this system discrete is to pull the states out of the system into a feedback loop.

$$\left[\begin{array}{c} \dot{x'} \\ \hline \dot{x_1} \\ \dot{x_2} \\ y_1 \\ y_2 \end{array}\right] = \left[\begin{array}{c|cc} \emptyset & I & \emptyset \\ \hline A_1 & \emptyset & B_1 \\ A_2 & \emptyset & B_2 \\ C_1 & \emptyset & D_1 \\ C_2 & \emptyset & D_2 \end{array}\right] \left[\begin{array}{c} x' \\ \hline \dot{x} \\ u \end{array}\right] \tag{6.4}$$

With the following feedback loop $\dot{x} = \theta_1 \dot{x_1} + \theta_2 \dot{x_2}$ and the general output is defined as $y = \theta_1 y_1 + \theta_2 y_2$.

If this system is made discrete, the states x_1 and x_2 are not affected as the discretisation algorithm will preserve the input-output behaviour. The discrete version of this system will look like this:

$$\left[\begin{array}{c} x'_{k+1} \\ \hline x_{1_k} \\ x_{2_k} \\ y_{1_k} \\ y_{2_k} \end{array}\right] = \left[\begin{array}{c|cc} I & I & \emptyset \\ \hline \theta_1 C_1 & \theta_1 D_{11} & \theta_1 D_{12} \\ \theta_2 C_2 & \theta_2 D_{21} & \theta_2 B_{22} \\ \theta_1 C_3 & \theta_1 D_{31} & \theta_1 D_{32} \\ \theta_2 C_4 & \theta_2 D_{41} & \theta_2 D_{42} \end{array}\right] \left[\begin{array}{c} x'_k \\ \hline x_k \\ u_k \end{array}\right] \tag{6.5}$$

with the feedback loop defined as: $x_k = x_{1_k} + x_{2_k}$ and the output as $y_k = y_{1_k} + y_{2_k}$.

This discrete system can still not be implemented as the static feedback loop and the non zero D_{11} and D_{21} matrices result in an algebraic loop. This algebraic loop has to be solved before implementation. To solve this loop for a fixed value of θ is not so difficult. In this case $\theta_1 C_1$ and $\theta_2 C_2$ merge to C_a, $\theta_1 D_{11}$ and $\theta_2 D_{21}$ merge to D_a and $\theta_1 D_{12}$ and $\theta_2 D_{22}$ merge to D_b. The system then simplifies to:

$$\left[\begin{array}{c} x'_{k+1} \\ \hline x_k \\ y_{1_k} \\ y_{2_k} \end{array}\right] = \left[\begin{array}{c|cc} I & I & \emptyset \\ \hline (I - D_a)^{-1} C_a & \emptyset & (I - D_a)^{-1} D_b \\ \theta_1 C_3 & \theta_1 D_{31} & \theta_1 D_{32} \\ \theta_2 C_4 & \theta_2 D_{41} & \theta_2 D_{42} \end{array}\right] \left[\begin{array}{c} x'_k \\ \hline x_k \\ u_k \end{array}\right] \tag{6.6}$$

With the feedback loop defined as: $x_k = x_{1_k} + x_{2_k}$ and the output as $y_k = y_{1_k} + y_{2_k}$.
And with: $C_a = \theta_1 C_1 + \theta_2 C_2$, $D_a = \theta_1 D_1 1 + \theta_2 D_2 1$ and $D_b = \theta_1 D_1 2 + \theta_2 D_2 2$.

If eq. 6.6 can be solved at each sample, this method can be used to implement the LPV controller in discrete time. The major limiting condition is that $(I - D_a)^{-1}$ has to be solved be solved each

sample. If that is possible, this method can easily be extended for LPV structures with more inputs and outputs or with a θ-vector.

A better solution to would be to solve the algebraic loop as a function of θ, though the $(I-D_a)^{-1}$-term makes this quite difficult. If the algebraic loop is solved, x_k has becomes a function of x_{k-1} and a non -linear function of θ. In case that this solution happens to be a 2^{nd}-order function of θ, the system can be rewritten to eq. 6.7. In other cases, list of H_i and K_i matrices has to be altered according to the order of the θ-dependency. This gives a more general solution to the discretisation problem. To prevent the list of H_i and K_i matrices, to become too large, the exact solution can be replaced by a lower order fit in θ.

Solving the algebraic loop for the system discussed in this thesis, shows that this relationship is approximately a 2^{nd}-order function of θ. So if eq. 6.6 is solved for various values of θ, a 2^{nd} order fit can be made to come to eq. 6.7

$$\left[\begin{array}{c} x'_{k+1} \\ \hline x_{1_k} \\ x_{2_k} \\ x_{3_k} \\ y_{1_k} \\ y_{2_k} \end{array}\right] = \left[\begin{array}{c|cc} I & I & \emptyset \\ \hline H_0 & \emptyset & K_0 \\ \theta H_1 & \emptyset & \theta K_1 \\ \theta^2 H_2 & \emptyset & \theta^2 K_2 \\ \theta_1 C_3 & \theta_1 D_{31} & \theta_1 D_{32} \\ \theta_2 C_4 & \theta_2 D_{41} & \theta_2 D_{42} \end{array}\right] \left[\begin{array}{c} x'_k \\ \hline x_k \\ u_k \end{array}\right] \tag{6.7}$$

with the feedback loop defined as: $x_k = x_{1_k} + x_{2_k} + x_{3_k}$.

To prevent algebraic loop errors caused by Matlab during the implementation, the other non-zero elements of the D-matrix are pulled out of the state space system, as shown in figure 6.5.

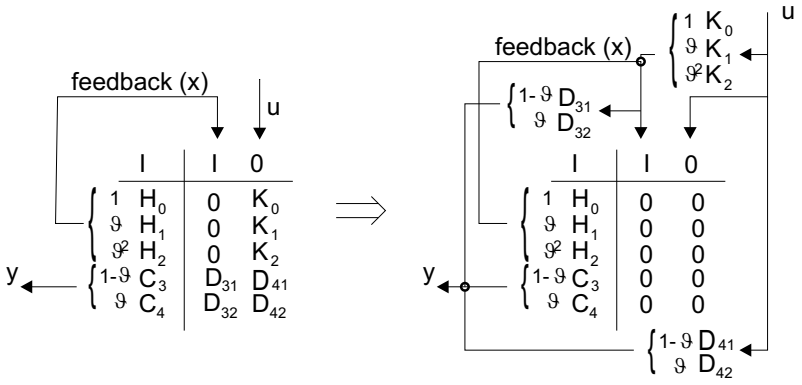

Figure 6.5: Implementation of the LPV controller

Figure 6.6 shows a LPV-controller and the discrete version of the controller using this method.

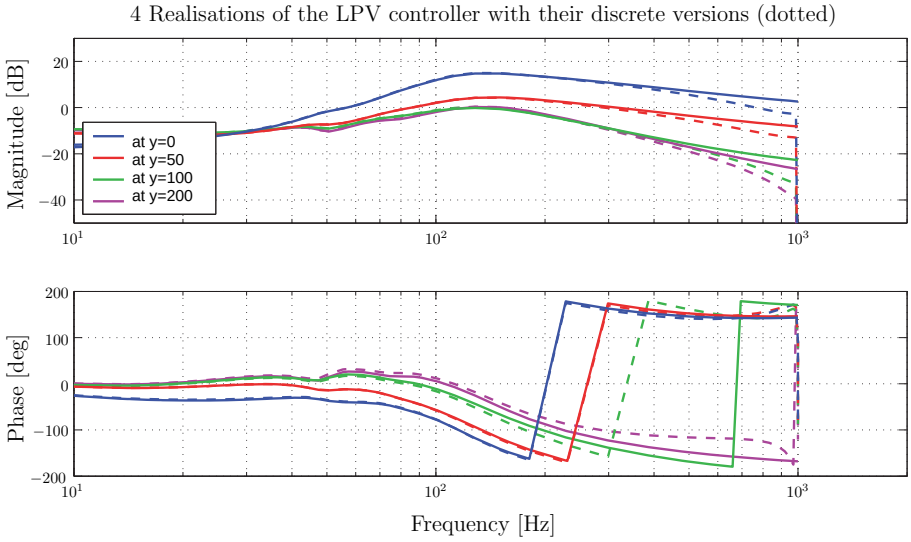

Figure 6.6: 4 Realisations of the LPV controller with their discrete versions (dotted)

6.5 Implementation

The LPV controller has a high high-frequent gain and it has too little phase margin (see Figure 6.4). During testing this results in noise amplification with a considerable frequency range. So a 2^{nd} order filter with a bandwidth of 100 Hz is added to the LPV controller and the gain is decreased to 75%. This improves the controller significantly. The noise peaks reduces to one dominant peak at the natural frequency of the system. This is similar to the $\mathcal{H}_\infty$ controller and the classical controller and is probably caused by amplification of the discretisation noise. A future solution could be to decrease the controller gain at that frequency by increasing the W_e filter at that frequency during the control design. Appendix C gives an overview of the noise peaks frequencies for the LPV controller with and without the filter. Appendix C gives an overview of the noise peaks for the different controllers.

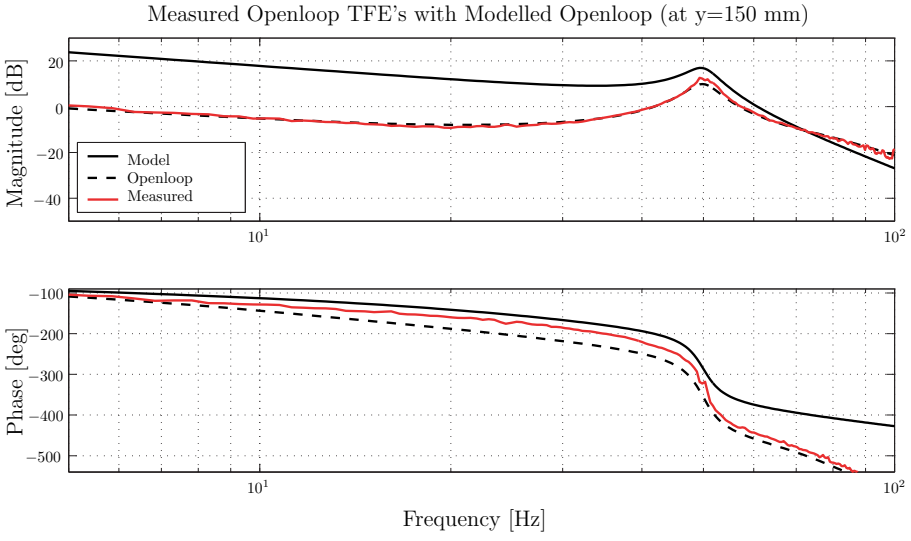

Figure 6.7: Measured LPV controller including a low-pass filter at $y = 190$ mm.

6.6 Conclusion

In this chapter a set of $\mathcal{H}_\infty$ controllers and an LPV controller are derived. The $\mathcal{H}_\infty$ controllers are only stable for a small rod position range. This results in a set of controllers that have a higher bandwidth than the classical controllers. The controllers use a notch filter to increase the bandwidth. The LPV controller should be able to combine these $\mathcal{H}_\infty$ controllers to one position dependent controller. The LPV controller, however, has a bandwidth comparable with the classical controller. This is the result of the robustness of the LPV controller to infinity fast position variations. This makes the controller more conservative the necessary. So in further research, the LPV controller should be derived with an algorithm that can derive a controller robust to limited position variations. Also manually combining the set of $\mathcal{H}_\infty$ controllers should lead to a less conservative LPV controller. The method described in chapter 3 can be used to derive such a controller.

To implement the LPV controller in discrete time, a discretisation algorithm is derived. The algorithm is only valid for the derived controller, but the discretisation method can also be used for other LPV models. The implemented LPV controller is too sensitive to high frequent measurement noise, so during implementation a 2^{nd} order filter is added to the controller. This has resulted in an implemented version of the LPV controller.

Part III

Further research and conclusions

Chapter 7

Two DOF system

This thesis describes the modelling and control design for a so called siso-system, a system with one input and one output. The next step in a hydraulic controller design is the modelling and control of a mimo-system with more inputs and outputs. This chapter describes a 2-input 2-output hydraulic system that can be used for further research.

7.1 Mimo general layout

This system has several new challenges in addition to those described for the siso system. In a mimo system one actuator can act on more degrees of freedom (dof). This means that movements in one dof will requires activity of more than one actuator. Also, the dynamics of the system can also be coupled. So the dynamics in one direction will also induce dynamics in other directions. In controller design this will lead to a mimo feedback loop instead of multiple siso feedback loops. All these couplings can be dependent on the working point of the system, which makes controller design even more difficult.

The system has different dynamic behaviour for different operating points. In its initial position the dynamics are decoupled. In other positions the actuators act on both dofs. Low frequent, this can be compensated by a static decoupling matrix. Also the dynamic behaviour is coupled, however if the system is only moved horizontally, only the rotation affects the translation acceleration and not the other way round. This means that a controller that controls the translation and the rotation can still be made out of two siso controllers. In other working points the dynamics are fully coupled and a mimo controller is required. If the system is not operated in a small region around one working point, both dynamics and coupling are position dependent. So also position-dependent controllers can also be evaluated.

7.2 Design

In the general layout (Figure 1.3 and 7.1) it is assumed that the system consists of two masses and that the hydraulic actuators act like springs. This gives a system with two natural frequencies causing the dynamic effects described in section 2. To ensure that these effects can be measured, the natural frequencies of the system should be below the bandwidth of the actuators. The internal stiffness of the components should also be high enough to make other natural frequencies higher than those of the described effects.

The available hydraulic cylinders for actuating are a MTS series 244 actuator for the rotational movement and a Parker Hannifin 2M series actuator for the horizontal movement. The servo valves mounted on the actuators have a bandwidth of approximately 100 Hz. The natural frequencies

of the system should be approximately 50 Hz to assure that the system can be actuated above these frequencies. For the stiffness given for both actuators the systems inertia that results in these natural frequencies can be calculated. For the vertical movement this is 220 kg and for the horizontal movement this is 110 kg (see table in the text). The horizontal actuator encounters the inertia from the mass of the system, the vertical actuator encounters the rotational inertia around point A. (See Figure 1.3). This rotational inertia should be 124 kgm^2 to assure that the vertical actuator encounters a virtual mass of 220 kg. To increase the rotational inertia, the design, depicted in figure 7.1, is chosen. The mass at the end of the triangle increases the rotational inertia.

MTS	Parker
$A = 13.5 \cdot 10^{-4}$ m^2	$A = 10.7 \cdot 10^{-4}$ m^2
$s = 250 \cdot 10^{-3}$ m	$A = 400 \cdot 10^{-3}$ m
$k = \frac{4AE}{s}$ and $\frac{1}{2\pi}\sqrt{\frac{k}{m}} = 50$ Hz give:	
$m = \frac{k}{(2\pi \cdot 50)^2} = 218.9$ kg	$m = \frac{k}{(2\pi \cdot 50)^2} = 108.4$ kg

The triangle has a mass (m) of 44 kg and a rotational inertia around point A (J_A) of 50 kgm^2. A mass of 34 kg at the end of the triangle will increase m till 78 kg and J_A till 125 kgm^2. If the weight of the sledge is increased till 32 kg both actuators encounters the right inertia. In the actual build system, the extra mass at the end of the triangle is increased till 40 kg. With a sledge weight increased till 26 kg this results in horizontal inertia off 110 kg and an inertia encountered by the vertical cylinder of 250 kg. This gives the following values for figure 7.1:

par.	value
m_1	26 kg
m_2	84 kg
J	33 kgm^2
α	2.5^o
l_1	1130 mm
l_2	750 mm
l_3	1050 mm

The second demand made on the natural frequencies of the system, is that the other natural frequencies of the system are higher than 50 Hz. To assure, the system is stiff enough to meet this requirement, the triangle has to be stiff enough. The natural frequency of the triangle is estimated by the natural frequency given by the stiffness of the triangle and the mass of 40 kg. This leads to a natural frequency of about 90 Hz.

7.3 The equation of motion

The modelling of this system can be devided into two parts. The first part consists of the hydraulic cylinders that can be copied from the 1-dof model. The second part consists of the equations of motion of the system. These are derived using Lagrange's method. (see de Kraker & van Campen [2001,p.74]; Wouw [2003,p.37-42] and Figure 7.1). Lagrange's method starts with positioning the masses in a global co-ordinate system.

$$\begin{aligned} \vec{r}_{OA} &= x_1 e_1^0 \\ \vec{r}_{OB} &= x_1 e_1^0 - l_1 e_1^1 \end{aligned}$$

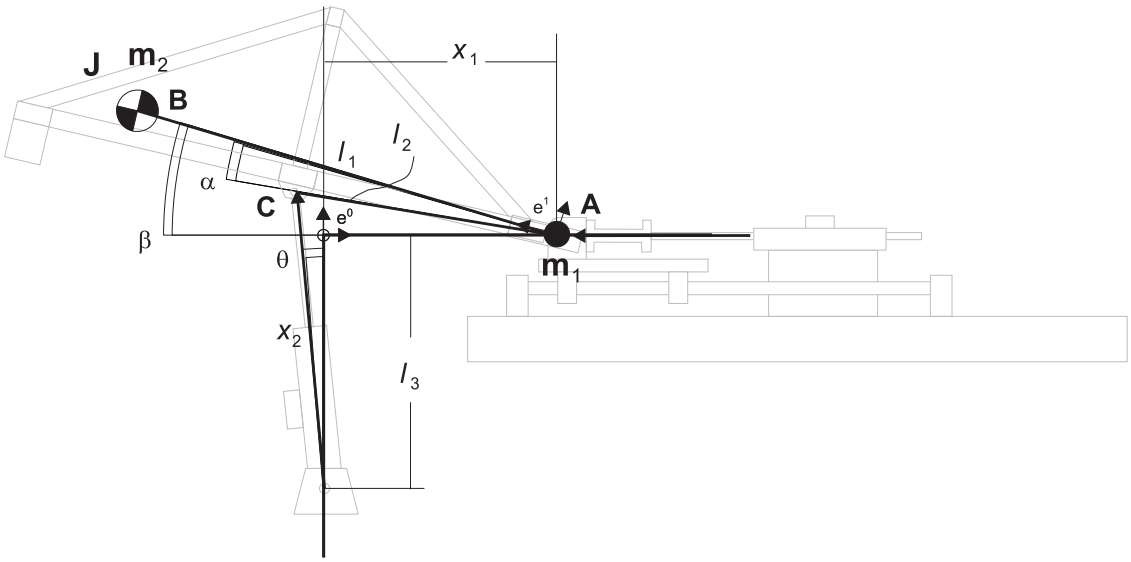

Figure 7.1: 2-dof system with measures for Lagrange's equations of motion

$$\begin{aligned} &= (x_1 - l_1\cos(\beta))\, e_1^0 + l_1\sin(\beta)e_2^0 \\ \vec{r}_{OC} &= x_1 e_1^0 - l_2\cos(\beta-\alpha)e_1^0 + l_2\sin(\beta-\alpha)e_2^0 \qquad (7.1) \\ &= (x_1 - l_2\cos(\beta-\alpha))\, e_1^0 + l_2\sin(\beta-\alpha)e_2^0 \end{aligned}$$

$$(7.2)$$

For this system these formula's are extended with formula's for the length x_2 and angle θ.

$$\begin{aligned} \theta &= \arctan\left(\frac{x_1 - l_2\cos(\beta-\alpha)}{l_2\sin(\beta-\alpha)+l_3}\right) \\ x_2 &= x_1^2 - 2x_1 l_2\cos(\beta-\alpha) + l_3^2 + l_2 l_3\sin(\beta-\alpha) \qquad (7.3) \\ \dot{x_2} &= -\dot{x_1}\sin(\theta) + \beta l_2\sin(\beta-\alpha+\theta) \end{aligned}$$

From these vectors the kinetic energy can be calculated:

$$T = \frac{1}{2}m_1\dot{\vec{r}}_{OA}\cdot\dot{\vec{r}}_{OA} + \frac{1}{2}m_2\dot{\vec{r}}_{OB}\cdot\dot{\vec{r}}_{OB} + \frac{1}{2}\vec{\omega}\cdot J\cdot\vec{\omega} \qquad (7.4)$$

$$= \underbrace{\frac{1}{2}(m_1+m_2)\dot{x}_1^2}_{\text{velocity}} + \underbrace{\frac{1}{2}(J+m_2 l_1^2)\dot{\beta}^2}_{\text{ang. velocity}} + \underbrace{m_2\dot{x}_1 l_1\sin(\beta)\dot{\beta}}_{\text{diff. velocity between } m_1 \text{ and } m_2} \qquad (7.5)$$

Second part is to define the systems states q, the external forces V and the non-conservative forces Q^{nc}:

$$\begin{aligned} q &= \begin{bmatrix} \vec{x}_1 & \beta \end{bmatrix}^T \\ V &= \begin{bmatrix} 0 & m_2 g l_1\sin(\beta) \end{bmatrix}^T \qquad (7.6) \\ Q^{nc} &= \sum_{i=1}^{n}\left(\frac{\delta\vec{r}_i}{\delta q}\right)^T\cdot F_i \\ &= \begin{bmatrix} F_1 - F_2\sin(\theta) \\ F_2 l_2\cos(\theta+\beta-\alpha) \end{bmatrix}_1 \end{aligned}$$

Now Lagrange's famous equation of motion can be be solved.

$$\frac{d}{dt}\left(\frac{dT}{d\dot{q}}\right) - \frac{dT}{dq} + \frac{dV}{dq} = Q_{nc}^{T} \tag{7.7}$$

$$\underbrace{(m_1+m_2)\ddot{x}_1}_{inertia} + \underbrace{m_2 l_1 sin(\beta)\ddot{\beta}}_{influence of \ddot{\beta}} + \underbrace{m_2 l_1 \cos(\beta)\dot{\beta}^2}_{centrifugal force} = \underbrace{F_1 - F_2\sin(\theta)}_{input} \tag{7.8}$$

$$\underbrace{(J+m_2 l_1^2)\ddot{\beta}}_{inertia} + \underbrace{m_2 l_1 \ddot{x}_1 sin(\beta)}_{influence of \ddot{x}} + \underbrace{m_2 g l_1 \cos(\beta)}_{gravity} = \underbrace{F_2 l_2 \cos(\theta+\beta-\alpha)}_{input} \tag{7.9}$$

In a matrix representation this looks like:

$$M(q)\ddot{q} + H(q,\dot{q}) = S(q)\tau$$

$$\begin{bmatrix} m_1+m_2 & m_2 l_1 \sin(\beta) \\ m_2 l_1 \sin(\beta) & m_2 l_1^2 + J \end{bmatrix}\ddot{q} + \begin{bmatrix} m_2 l_1 \cos(\beta)\dot{\beta}^2 \\ m_2 g l_1 \cos(\beta) \end{bmatrix} = \begin{bmatrix} 1 & -sin(\theta) \\ 0 & l_2\cos(\theta+\beta-\alpha) \end{bmatrix}\begin{bmatrix} F_1 \\ F_2 \end{bmatrix} \tag{7.10}$$

7.4 Linearisation

The derived equations of motion are obviously nonlinear, as was demanded for the system. For control design, linearised models are required. Even several nonlinear control strategies, such as LPV controllers, are based on a set of linear controllers based on linear models.

Therefore, a linearised model is derived [see de Kraker & van Campen 2001,p.105]. This model is of course dependent on it position (x_0, β_0):

$$\begin{aligned}
M_{lin} &= M(q_0) &&= \begin{bmatrix} m_1+m_2 & m_2 l_1 sin(\beta_0) \\ m_2 l_1 sin(\beta_0) & m_2 l_1^2 + J \end{bmatrix} \\
D_{lin} &= \tfrac{\delta H}{\delta \dot{q}}(q_0)\dot{q}_{lin} &&= \begin{bmatrix} 0 & 0 \\ 0 & 0 \end{bmatrix} \\
K_{lin} &= \tfrac{\delta H}{\delta q}(q_0)q_{lin} + \tfrac{\delta S(q)\tau_{lin}}{\delta q}(q_0)q_{lin} &&= \begin{bmatrix} 0 & 0 \\ 0 & F_2 l_2 \sin(\theta_0+\beta_0-\alpha_0) \end{bmatrix} \\
S_{lin} &= S(q_{lin}) &&= \begin{bmatrix} 1 & -sin(\theta_0) \\ 0 & l_2\cos(\theta_0+\beta_0-\alpha_0) \end{bmatrix}
\end{aligned}$$

$$M_e\ddot{q} + D_e\dot{q} + K_e = S_e F \tag{7.11}$$

7.5 Modelling

With the derived equations of motion and the model for a hydraulic actuator derived in chapter 2 all components of the mimo system are modelled. Two models can be derived, a linear and nonlinear, from these components. With the nonlinear functions, a nonlinear model is made in Matlab Simulink. With the linearised functions, a linear set of linear transfer functions is made for different working points. The models can be compared with the actual built system.

Figure 7.2 shows the working range of the mimo system. Figure **??**a and b depict the linearised dynamics of this nonlinear model around different working points. This figure is made with incorrect cylinder stiffness so the natural frequencies are not at the designed frequency.

Figure 7.3 shows that the highest natural frequency is dependent on the horizontal movement. The lowest natural frequency is independent on the horizontal movement. So the highest natural

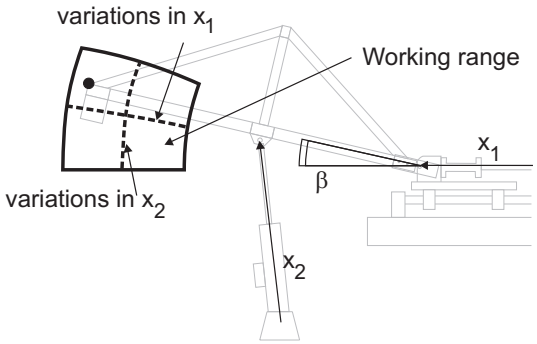

Figure 7.2: The working range of the mimo system. The dotted lines depict two position variations. One in the horizontal direction and one in the vertical direction.

Transfer function from the horizontal input (u_1) to the to the displacement (x) of the system at $x_2 = 1.075$ m for different x_1

Transfer function from the vertical input (u_2) to the to the rotation (β) of the system at $x_2 = 1.075$ m for different x_1

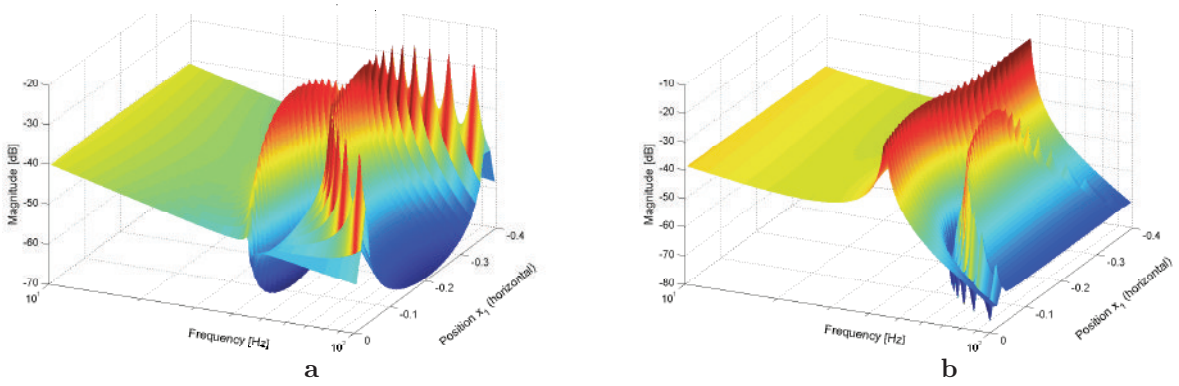

Figure 7.3: **a** depict the horizontal transfer function at $x_1 = 0.2$ m as a function of the vertical position. **b** depict the vertical transfer function at $x_1 = 0.2$ m as a function of the vertical position. The transfer functions from vertical input to horizontal output and vice versa are not depicted.

frequency will be the natural frequency of the horizontal actuator and the lowest natural frequency will be the natural frequency of the vertical actuator. Variations in the horizontal direction do have a little effect on the lowest natural frequency, as the angle of attack of the vertical actuator differs for different horizontal positions.

Chapter 8

Conclusions and recommendations

The aim of this study was to compare different controllers for a hydraulic servo system. Hydraulic actuators have considerable position dependent behaviour, so the comparison focused on the methods used by the different controllers to cope with this nonlinearity. To achieve this, a model has been made of an asymmetric hydraulic actuator. Based on this model, a classical controller, a $\mathcal{H}_\infty$ controller and a LPV controller were designed and implemented. For the implementation of the LPV controller a new discretisation algorithm was written. Furthermore a mimo system was built to be able to extend this study to mimo hydraulic systems.

8.1 Conclusions

8.1.1 Modelling

To improve the insight in the system, a white box model was derived using a physical description of the system. This model was linearised except for its position depend behaviour. This model also gave a good indication where to focus on during black box model fits, such as its dependency on the rod position. This shows the benefit of white box modelling used next to black box modelling.

Black box, 'pole zero' models were fitted on measured transfer functions. Four models were fit for four different rod positions. During the fit procedure, it was assured that only one complex pole pair varied for the four models. This showed that insights derived from the white box model could improve the black box fits. Furthermore, using the white box model, the physical background of the different poles and zeros could be derived.

At last a LPV model was derived. This was achieved by fitting the varying parameters of the black box models linearly on a predefined nonlinear function of the position. This nonlinear function was derived from the white box model. This showed that an LPV model could be fitted on measured transfer function data. Furthermore its showed that the insights from the physical model of the system could help to improve the fit procedure.

8.1.2 Control

During the controller design local controllers were designed, which are only stable for a small position range. Also global controllers were derived, which are stable for all positions. The local and global controllers were designed using both a classical loop shaping approach and a $\mathcal{H}_\infty$ approach. Also an LPV controller was designed that should be able to make a global scheduling controller similar to the set of local $\mathcal{H}_\infty$ controllers.

The global $\mathcal{H}_\infty$ controllers did not have better performance than the classical controllers because

the plant uncertainty, due to the position dependent natural frequency, is too high. This prevented the $\mathcal{H}_\infty$ algorithm to find a more specific control approach with more bandwidth than the classical control approach. This leads to the conclusion that the classical control approach is an optimal linear control approach for the described hydraulic actuators.

Local $\mathcal{H}_\infty$ controllers had been designed for a smaller working range that led to a smaller plant uncertainty. The derived controllers use a notch filter to increase the bandwidth. The LPV controller, that should have combined these controllers to one position dependent controller, had a much lower bandwidth than the set of local $\mathcal{H}_\infty$ controllers. Apparently the LPV controller could not combine the local $\mathcal{H}_\infty$ controllers. This was the result of the used algorithm that makes the LPV controller robust for infinity fast changes in the position. Since those fast changes cannot occur, the LPV controller was too conservative. This leads to the conclusion that for hydraulic servo control, LPV algorithms cannot be used since they are too conservative.

This leads to the general conclusion that, at this point, the classical hydraulic control approach gives the best performance. The local controllers, however, performed much better then the global controllers. So the conclusion can be drawn that improving the LPV controller is worth trying since this approach can combine the local controllers. The LPV controller can be improved by making it less robust for fast changes in the position. This requires the use of an algorithms that is not only parameter dependent, but also dependent on the derivative of the parameter.

Besides the conclusions on the comparison of the different control approaches, it should be noted that the low phase of the servo valve and the low bandwidth of the position sensor have a limiting effect on the bandwidth of all controllers.

8.1.3 MIMO system

For further research on hydraulic control, a mimo-system has been designed and built. This system has two hydraulic actuators. The mass of this system was chosen relative large compared to the stiffness of the actuators. So the mimo-system had low natural frequencies compared to the bandwidth of the servo valves. This low natural frequency enabled the design of controllers that compensate for this shifting natural frequency, without being hindered by limitations due to the servo valve.

The system was designed in such a way that the coupling of the dynamics of the system varies for different positions. This resulted in a system with no coupled dynamics at the base position and considerable coupling at the most extended position. This will enable the design of: 1) Two siso-controllers for the non coupled position. 2) The design of a mimo-controller for a coupled position. 3) The design of a varying mimo-controller that is valid for all positions.

So a new set-up is designed and build that can be used for research on control design for mimo systems with adjustable coupling between the degrees of freedom and for mimo systems with position dependent coupling between the degrees of freedom.

8.2 Recommendations

8.2.1 Control

The bandwidth of the position sensor should be increased. A possible way is by combining the position sensor measurements with acceleration measurements.

To derive LPV controllers that are less robust to fast position changes, algorithms should be used that are not only parameter dependent, but also dependent on the derivative of the parameter. Another approach is manually fitting the varying parameters of the notch filters, used in the local $\mathcal{H}_\infty$ controllers to one varying notch filter. The model multiplied with this varying notch filter gives a position independent model. For this model a $\mathcal{H}_\infty$ controller can be designed. This

approach leads to a gain scheduling controller, derived by hand. This approach is of course similar to an input output linearisation approach.

8.2.2 MIMO system

The mimo system is much heavier then the siso system. So comparable forces result in smaller displacements. Better position sensors are required for the mimo system than for the siso system. In the appendices a method to improve the position estimate with acceleration measurements is described.
Before designing a controller, the system dynamics should be decoupled. This decoupling should be position dependent. This thesis presents the equations of motion of the mimo system and a model for a hydraulic actuator. If those are combined, a decoupling can be derived for different positions.

Bibliography

Apkarian, P. "On the Discretization of LMI-synthesized Linear Parameter-varying Controllers", 1997, Automotica, 655

Damen, A. & Weiland, S. "Robust Control, lecture notes", 2002, Eindhoven University of Technology, Department of Electrical Engineering, Measurement and Control Group

de Kraker, B. & van Campen, D. 2001, "Mechanical Vibrations" (Maastricht NL: Shaker Publishing), 1^{th} edition

DIET 2005, DIET, Eindhoven University of Technology, Department of Mechanical Engineering, Control Systems Technology Group, do It Easy Toolbox

dSpace Inc. 2005, dSpace control board, (http://www.dspaceinc.com/ww/en/inc/products.htm)

Franklin, G., Powell, J., & Emani, A. 1993, "Feedback Control of Dynamic Systems" (New York US: John Wiley & Sons Inc.), 3^{th} edition

Koekebakker, S. 2001, "Model based control of a flight simulator motion system" (Delft NL: Delft University of Technology), 1^{th} edition

MCDesign. 2005, MCDesign, Eindhoven University of Technology, Department of Mechanical Engineering, Control Systems Technology Group, Naus, G.J.L. & Wijnheijmer, F.P. (http://www.simonstevin.tue.nl/MCDesign)

Merrit, H. 1967, "Hydraulic Control Systems" (New York US: John Wiley & Sons Inc.), 1^{th} edition

MOOG. 2005, MOOG 76-233 servo valve (http://www.moog.de)

MTS. 2005, temposonic Position sensor (http://www.mtssensor.de/produkte/temposonics.html)

Paine. 2005, pressure sensor 3000 PSID (http://www.paineelectronics.com/refchart.htm)

Post, W. & Teerhuis, P. 2005, "Hydraulic Servo Control, lecture notes", Eindhoven University of Technology, Department of Mechanical Engineering, Control Systems Technology Group

Rexroth. 2005 (http://www.boschrexroth.com/country_units/europe/netherlands/nl/systems_engineering/training/hydra

Sastry, S. 1999, "Nonlinear Systems" (DE: Berlin: Springer), 1^{th} edition

Scherer, C. & Weiland, S. 2005, "Linear Matrix Inequalities in Control", 1^{th} edition

Sirouspour, M. & Salcudean, S. "On the Nonlinear Control of Hydraulic Servo-systems", 2000, The University of British Columbia

Sohl, G. & Bobrow, J. "Experiments and Simulations on the Nonlinear Control of a Hydraulic Servosystem", 1999, IEEE Transactions on control systems technology, 7, 238

Sugiyama, T. & Uchida, K. "Gain Scheduled Velocity and Force Controllers for the Electro-hydraulic Servosystem", 2002, IEEE Proceedings of the American control conference, 6, 4433

Trangbæk, K. 2001, "Linear Parameter Varying Control of Induction Motors" (Aalborg DK: Centertrykkeriet, Aalborg University), 1^{th} edition

Viersma, T. 1990, "Analysis, Synthesis and Design of Hydraulic Servosystems and Pipelines" (Delft University of Technology), revised edition

Voort, A. V., Steinbuch, M., & Molengraft, R. V. "Experimental modelling and LPV Control of a Motion System", 2003, IEEE Proceedings of the American control conference, 1374

Wassink, M. G., van de Wal, M., Scherer, C., & Bosgra, O. "LPV control for a wafer stage: beyond the theoretical solution", 2005, Elsevier Control engineering practice, 13, 231

Wouw, N. 2003, "Multibody Dynamics, lecture notes", Eindhoven University of Technology, Department of Mechanical Engineering, Control Systems Technology Group

Yao, B., Bu, F., & Chiu, G. "Non-linear adaptive robust control of electro-hydraulic systems driven by double-rod actuators", 1999, IEEE Proceedings of the American Control Conference, 6, 759

Yun, J. & Cho, H. "Adaptive model following control of electro hydraulic velocity control systems subjected to unknown disturbances", 1988, IEEE Proceedings, 135, 149

Appendix A

Matlab tools

This appendix gives an overview of the functions used for this research. The actual functions are stored on the CD-rom disk supplied with this thesis.

Besides the here described functions, the MCDesign toolbox [MCDesign 2005] and the Diet toolbox [DIET 2005] are used for this research.

A.1 Simulink simulation files

sim_01m.m Performs time simulations on the 1 dof model `sim_01.mdl` using parameter values defined in the function.

sim_02m.m Performs time simulations on the 2 dof model `sim_02.mdl` using parameter values defined in the function.

A.2 $\mathcal{H}_\infty$ control functions

test_midden.m Derives the δP filter by comparing the black box models.

hinfsyn_oplossinga.m Calculates the position $\mathcal{H}_\infty$ controller using the initial filters and plots the results.

hinfsyn_oplossingb.m Calculates the position $\mathcal{H}_\infty$ controller using the final filters and plots the results.

hinfsyn_oplossingc.m Calculates the position and pressure $\mathcal{H}_\infty$ controller using the final filters and plots the results.

A.3 LPV control functions

makeaffine.m Performs both the fits required to derive the fit of the θ-function on the position and the LPV model fit on the black box models.

make_theta.m Calculates θ for a given rod position for the relation between the position and θ derived in `makeaffine.m`.

LPV2ss.m Derives a state space representation of a polytopic LPV model for a certain value of θ.

LPV_oplossing_hinf.m Calculates the set of local $\mathcal{H}_\infty$ controllers and a LPV controller from the weighting functions tuned for $\mathcal{H}_\infty$ controller, which are also defined in this function. The file uses the LPV model and uncertainty defined in `overzich_LPVfits.mat`.

LPV_oplossing_low.m Idem, for only, this function uses the filters tuned for the LPV controller.

LPVc2d.m This function converts the continues LPV controller to a discrete time version. The used method is described in chapter 6. The files `LPVdemo.mdl` and `LPVdemo_R11.mdl` give a demonstration of the implementation of the derived LPV controller.

A.4 Simulation functions for the 2 dof model

sim_02_settings.m This file loads actual the parameter values required for all calculations on the 2 dof system.

dof2_lin.m Derives a linearisation of the nonlinear Lagrange's equations of motion of the 2 dof system around a working point (x,β).

dof2_vars.m Completes the list $[x_1, \beta, x_2, \theta]$ if two of the entries are given (see chapter 7).

check_overdrachten.m This file uses `dof2_lin.m` to linearise the equations of motion around a certain working point and couples the linear model to linearised models of the two hydraulic actuators and the servo valves.

control_overdrachten.m This files uses `check_overdrachten.m` to calculate the linearised model of the 2 dof system and adds a controller to this system.

lpv_diff_systems.m This files derives linearisations using `check_overdrachten.m` for a grid of working points.

show_lpv_diff_systems.m Plots 3D transfer functions from the data calculated with `lpv_diff_systems.m`.

A.5 Functions to plot the results depicted in this report

plot_different_controllers.m Plots the controllers and open loop responses depicted in this report.

plot_measured_transfers.m Calculates and plots the measured transfer function estimates from the original data files.

plot_whitebox_extra_data.m Plots the extra measurements performed to fit the white box model from the original data files.

Viewtreeentries.m Plots the results from the LPV model fit on the parameter θ.

Appendix B

MCDesign

Various tools like DIET (Do It Easy Tool) [DIET 2005] and the SISOtool of Matlab exist for control design using loop shaping techniques. Most of these tools are developed for control design for siso systems. For mimo loop shaping no appropriate tool available. Therefore MCDesign (MIMO Control Design) [MCDesign 2005] was developed by G.J.L. Naus and F.P. Wijnheijmer to facilitate working with these systems and models.

MCDesign uses the Matlab environment and consists of three main parts. The dtf-data object, which facilitates working with measurement data. Calculation with siso as well as mimo data and models is reduced to summation, multiplication, et cetera of the dtf object. CDesign is a tool to apply loop shaping and pole-zero placement techniques to siso systems. Using CDesign, controllers can be designed as well as black box fits of measurement data can be made. MDesign is the command window controlling the data, especially suited for MIMO systems. In the main window, the various transfer functions of the system are shown from where controllers, fits of the data, et cetera can be designed. To simplify importing measurement data into MDesign, SDesign is developed. SDesign is a tool to convert measurement input output data to data-based transfer functions, which can be imported into MDesign. In the near future among other things, also mimo system data fitting, which signifies grey box fitting with fixed poles as well as $\mathcal{H}_\infty$ control will be implemented.

For a thorough description of the MCDesign tool, see the MCDesign Manual MCDesign [2005].

Appendix C

Noise reduction for LPV control

After the implementation of the LPV controller, controlled system vibrates high frequent. To find the cause of this high frequent noise peaks, a the power spectrum of the measured position signal is plotted for various controller conditions (see Figures).

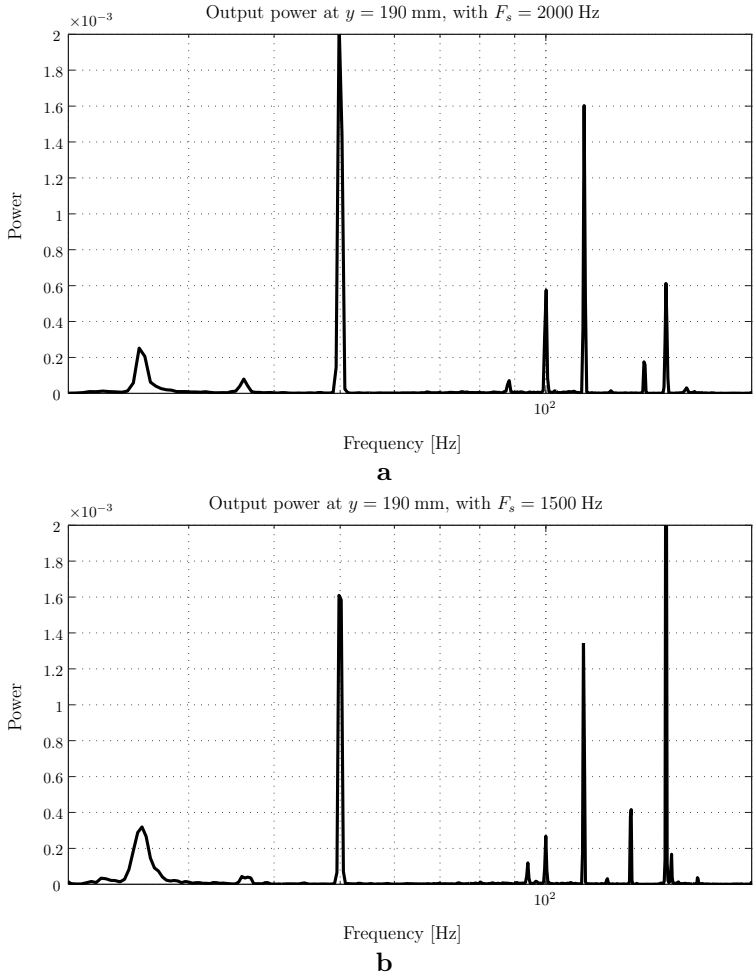

Figure C.1: Power spectrum of the position measurement at $y = 190$ mm. **a:** $F_s = 2000$ Hz and **b:** $F_s = 1500$ Hz.

The spectrum can have various causes, but the most likely causes are aliasing of high frequent sensor signals or amplification of measurement noise by the high frequent gain of the LPV controller. To test whether the noise peaks are caused by aliasing, the power spectrum is measured for different sample frequencies (see Figure C.1a and b). As the spectrum does not change for different sample frequencies, the noise is not caused by aliasing.

The spectrum is also measured for a different position (see Figure C.2). At a different position both the controller and the system are different. Except for the 50 Hz and 100 Hz component, probably caused by the power net, this results in a different noise spectrum. So the noise is probably caused by the interaction between the system and the controller.

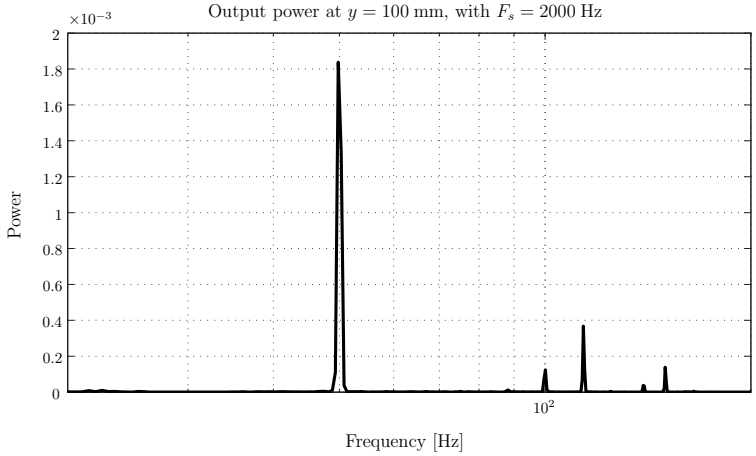

Figure C.2: Power spectrum of the position measurement at $y = 100$ mm, with $F_s = 2000$ Hz.

After applying a 2^{nd}-order low pass filter, the noise spectrum reduces to a single peak at 50 Hz (see Figure C.3). As removing the high frequent component of the controller reduces the noise, it can be concluded that the noise was caused by the high frequent gain of the LPV controller.

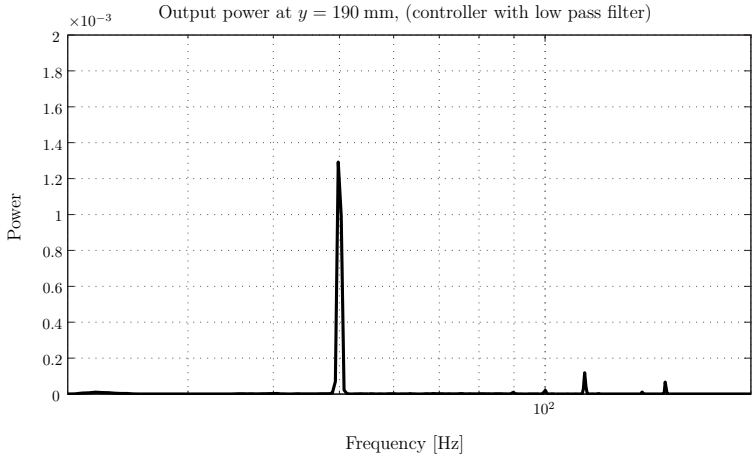

Figure C.3: Power spectrum of the position measurement at $y = 190$ mm, (controller with low pass filter).

Appendix D

Acceleration as a position sensor

Figure D.1 shows that the used position sensors dynamic behaviour is limited. The sensor has the effect of a first order filter with a pole at 45 Hz. Furthermore, it has considerable high frequent noise. To increase the dynamic range and accuracy of the position measurement, an acceleration measurement can be used. Theoretically, the second integral of the acceleration results in a position estimate. In practice, even a small DC-offset in the acceleration measurement results in a quadratic drift of the position estimate, so the acceleration measurement should be corrected for this effect. This can be achieved by feedback of the error between the position estimate and the position measurement. The created feedback loop consists of the two integrals which makes it unstable. So another approach is chosen.

This approach is depicted in figure D. In this approach the acceleration measurement is integrated two times by a 2^{nd} order low pass filter. The low pass filter prevents the integrators from saturating if the acceleration sensors have a DC-offset. Low frequent errors in the integrated acceleration signal are suppressed by the feedback loop. The feedback loop consists of an integrator in stead of a gain to assure that the feedback loop only suppresses low frequent signals. The gain G is the feedback gain.

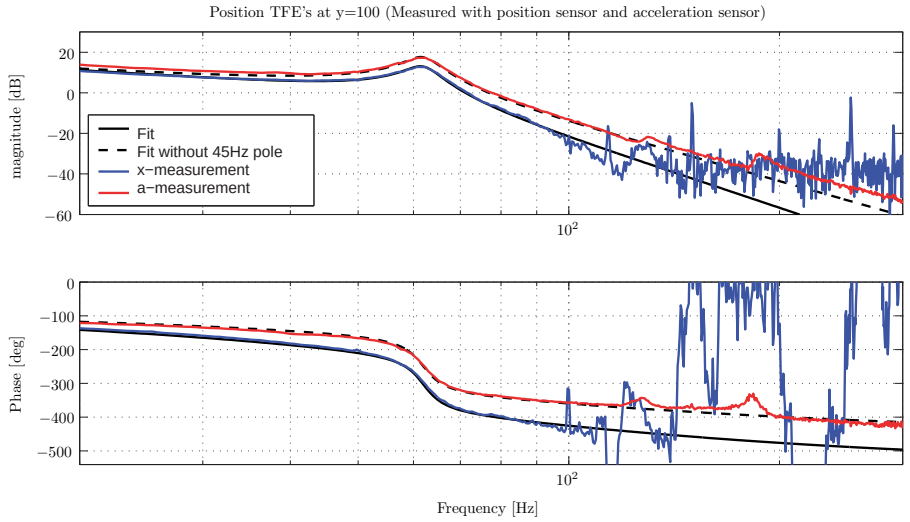

Figure D.1: Comparison of the position transfer function estimate based on the position sensor and based on the acceleration sensor.

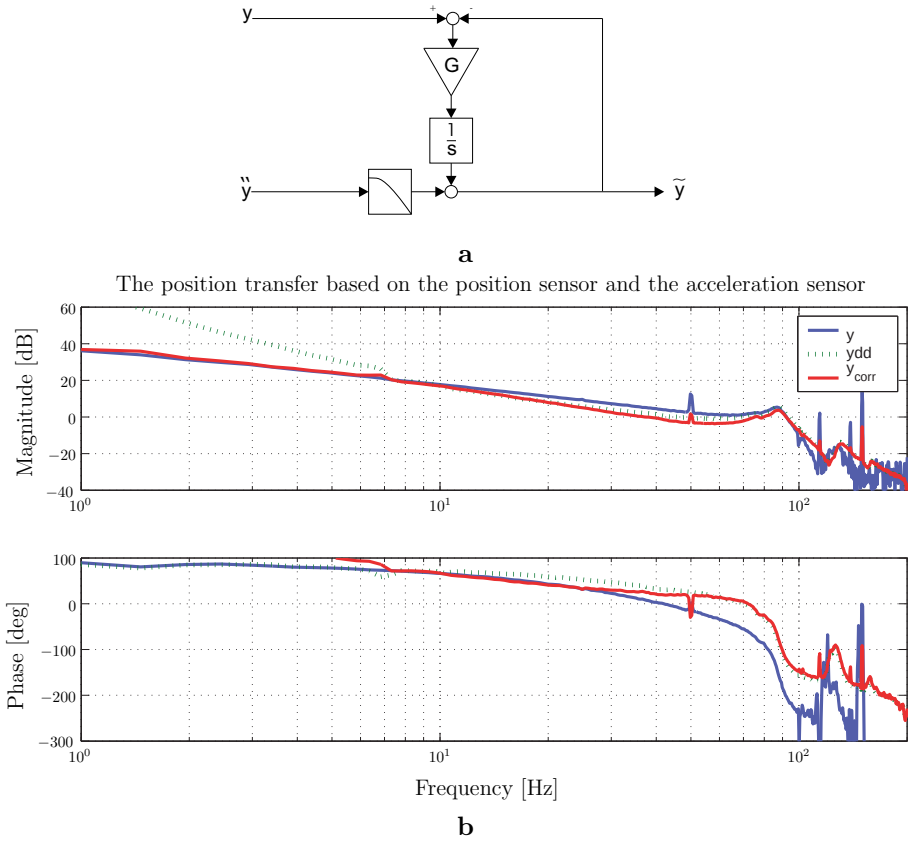

Figure D.2: The used filter to include acceleration measurements in the position estimate.
a: The used filter, **b:** the resulting transfer functions estimates (tfe) for the position transfer. The light line is the original tfe measured with the position sensor and has bad high frequent accuracy. The dotted line is measured with the acceleration sensor and has a bad low frequent magnitude. The solid line is derived with the estimate explained in the chapter.